FINAL REPORT FOR USGS AWARD NUMBER G12AP20098

INFLUENCE OF LIQUEFACTION ON EARTHQUAKE GROUND MOTIONS

Principal Investigators:

Scott J. Brandenberg, Ph.D.
Associate Professor and Vice Chair
Department of Civil and Environmental Engineering
5731 Boelter Hall
University of California, Los Angeles, CA 90095-1593
phone: 310-825-9819; fax: 310-206-2222; email: sjbrandenberg@ucla.edu

Jonathan P. Stewart, Ph.D., P.E.
Professor and Chair
Department of Civil and Environmental Engineering
5731 Boelter Hall
University of California, Los Angeles, CA 90095-1593
phone: 310-206-2990; fax: 310-206-2222; email: jstewart@seas.ucla.edu

Graduate Student Researcher:

Kamil B. Afacan
Department of Civil and Environmental Engineering
University of California, Los Angeles

Term covered:
July 1, 2012 - December 31, 2013

Contents

Abstract 3
1 Total Stress Site Response Modeling of Soft Clay Centrifuge Models 4
1.1 Adjusting Modulus Reduction Curve to Provide Desired Shear Strength 8
1.1 Correction of Shear Strength for Strain Rate Effects 11
1.2 Site Response Modeling Analyses 14
1.3 Site Response Modeling Results 17
1.3.1 Influence of Undrained Shear Strength 17
1.3.2 Comparison of DeepSoil and OpenSees 21
1.3.3 Comparison of Nonlinear and Equivalent Linear Simulations 24
1.3.4 Influence of strain rate correction 27
1.3.5 Residuals of Various Ground Motion Intensity Measures 30
2 Effective Stress Nonlinear Site Response Analysis of Centrifuge Models Involving Liquefaction 32
2.1 Measurement of Acceleration Pulses in Liquefied Sand 32
2.2 Explanation of Acceleration Pulses in Liquefied Sand 34
2.3 Pore Pressure Generation Models 35
2.4 Advanced Constitutive Models 38
2.5 Description of Centrifuge Model CSP3 40
2.6 Site Response Modeling 41
2.7 Comparison of Site Response Simulations with Measured Results 43
3 Summary and Conclusions 49
4 Acknowledgments 51
5 References 51

Abstract

Research project G12AP20098 "Influence of Liquefaction on Earthquake Ground Motions" covers two principal topics related to nonlinear site response: (1) total stress simulations of centrifuge models involving soft clay that were strongly shaken in a previous USGS-funded research study, and (2) effective stress simulations of centrifuge models including liquefiable sand layers. Primary conclusions from the total stress analysis are (1) unreasonable shear strength values may arise from extrapolating modulus reduction curves to large strains, and properly modeling the shear strength by adjusting the high-strain region of the modulus reduction curve is essential for accurate nonlinear site response modeling, and (2) the shear strength must be adjusted for strain rate effects to capture the measured ground motions. The primary conclusion from the effective stress simulations is that ground motions following liquefaction triggering are significantly under-predicted using a modeling procedure in which the backbone stress-strain behavior is degraded as pore pressures develop in accordance with a pore pressure generation function. These models fail to capture the dilatancy behavior of liquefied sand that manifests as a transient stiffening in undrained loading, and enables propagation of high amplitude high frequency acceleration pulses. Use of such models for predicting ground motions in liquefiable soils should therefore be avoided, although these models are capable of predicting liquefaction triggering in some cases. More sophisticated constitutive models capable of capturing the dilatancy behavior are demonstrated to have the capability to replicate these acceleration pulses, but the resulting ground motions are highly sensitive to input parameters. More research is needed to calibrate and validate these advanced constitutive models.

1 Total Stress Site Response Modeling of Soft Clay Centrifuge Models

A pair of centrifuge tests were performed at the nees@UCDavis 9m radius geotechnical centrifuge facility as part of a previously-funded USGS study (project number 08HQGR0037). The scope of the previous study was to perform the centrifuge tests and archive the experimental data, but the budget and timeline was inadequate to perform site response simulations for comparison with the experimental data. The site response studies are therefore included in this report. This report does not present all of the details of the centrifuge modeling study, which have been well documented by Afacan et al. (2013) and Brandenberg et al. (2010). Rather, we focus this report on site response modeling of these centrifuge models, and include a few relevant details from the centrifuge modeling for the purpose of making meaningful comparisons with the site response simulations.

Two centrifuge models, denoted AHA01 and AHA02, were composed of a layer of sand overlying a lightly overconsolidated layer of San Francisco Bay mud overlying a more heavily overconsolidated deposit of bay mud (Fig. 1). The bay mud layers were separated by thin layers of sand to provide drainage conditions during consolidation of the clay from slurry and during centrifuge spinning. Profiles of vertical effective stress, consolidation stress, shear wave velocity, and undrained shear strength are shown in Fig. 2.

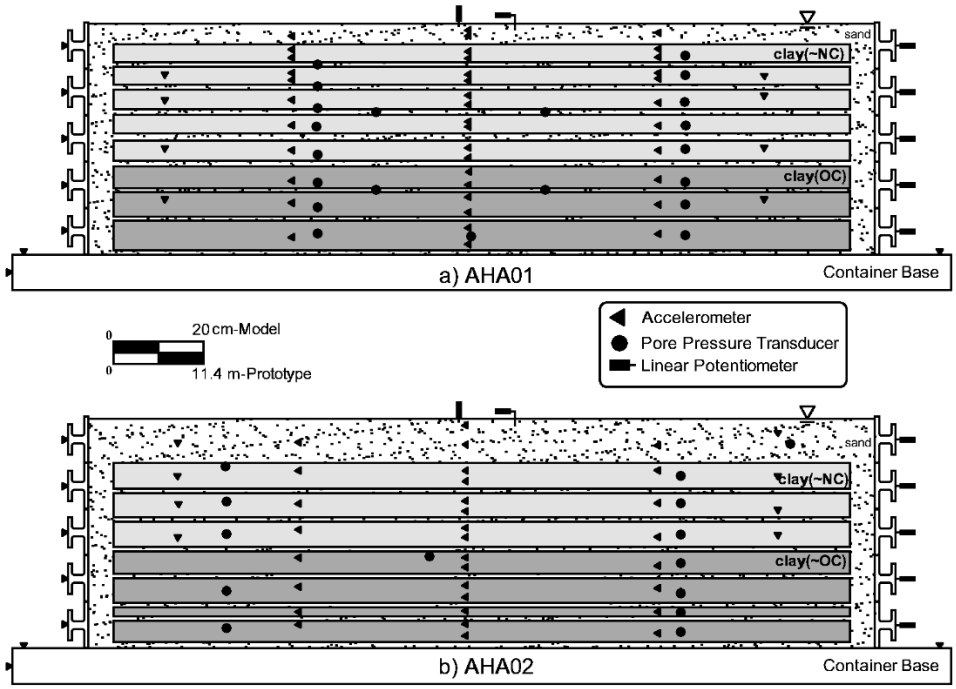

Figure 1. Sketches of centrifuge model (a) AHA01 and (b) AHA02 (Afacan et al. 2013).

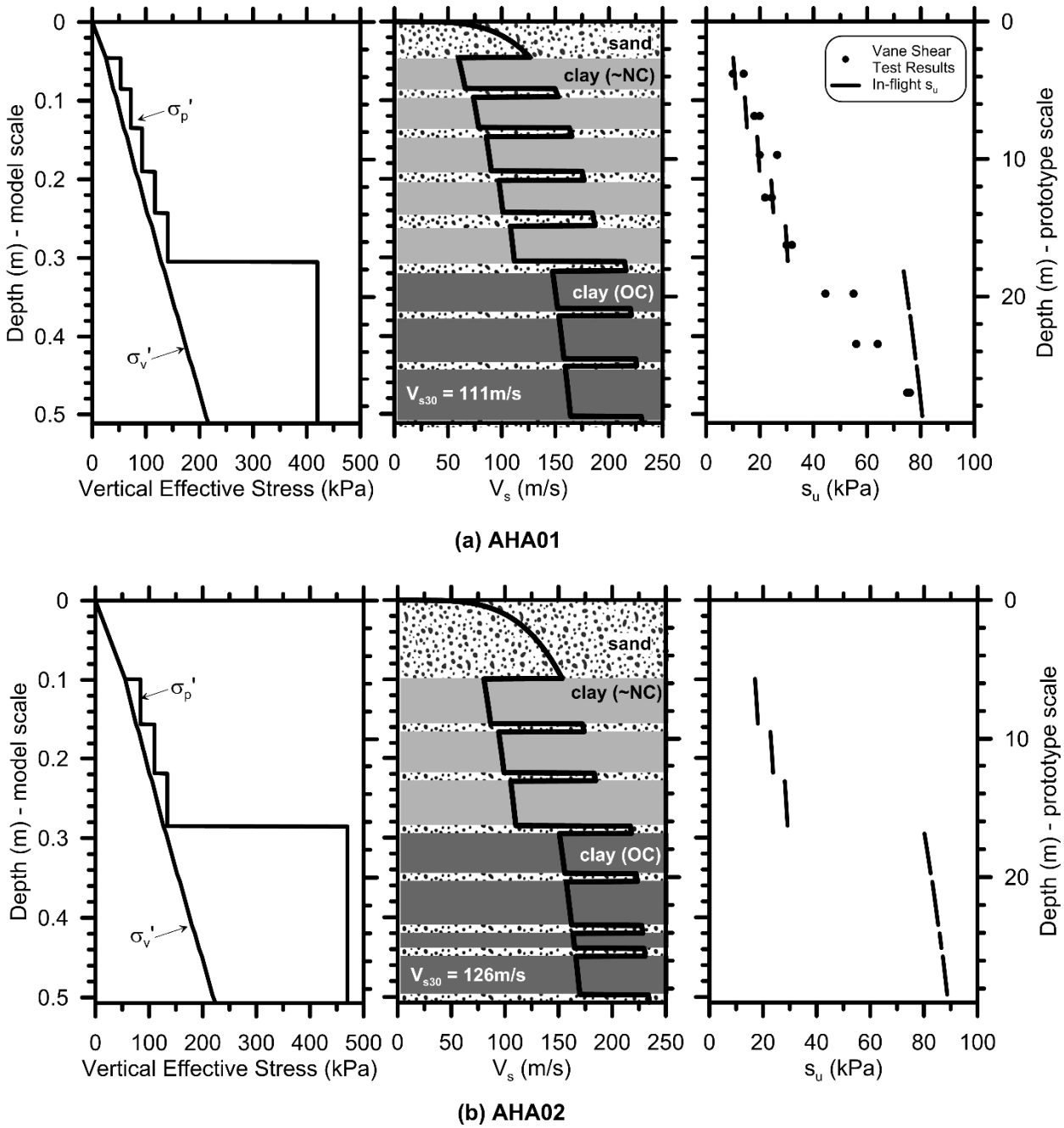

Figure 2. Profiles of vertical effective stress, consolidation stress, shear wave velocity, and monotonic undrained shear strength for centrifuge model (a) AHA01 and (b) AHA02 (Afacan et al. 2013).

The models were shaken by a sequence of ground motions ranging from very small amplitude events exciting the models essentially within their linear elastic range, to very high amplitude events that generated shear strains in excess of 10% in some layers, essentially corresponding to a failure condition

of the clay. Acceleration response spectra of the motions recorded near the base of the centrifuge models are shown in Fig. 3. The range of peak acceleration imposed on the base of the models was 0.02g to 0.6g. Weak motions were amplified by the soil profile, whereas stronger motions were de-amplified, as shown in Fig. 4.

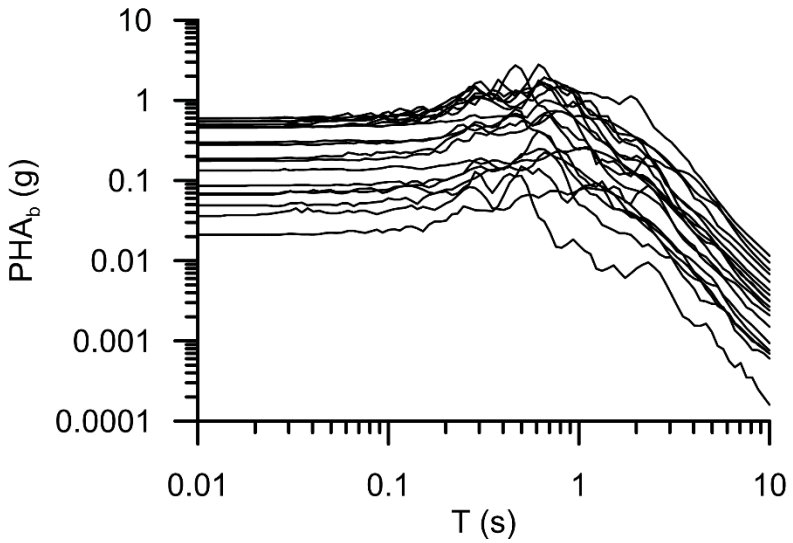

Figure 3. Acceleration response spectra of base motions recorded during centrifuge models (5% damping).

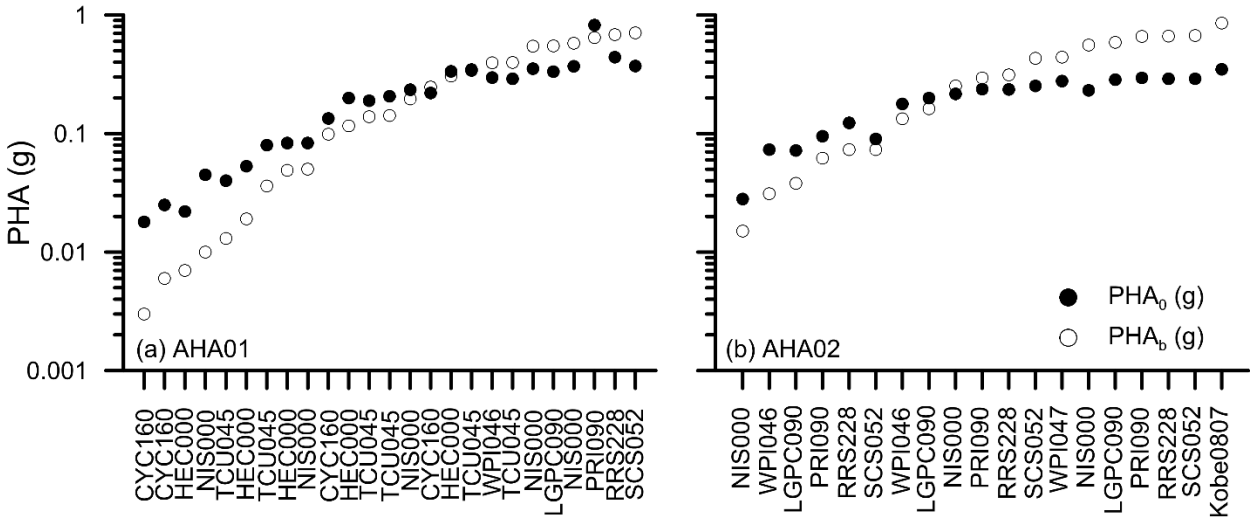

Figure 4. Beak base acceleration and peak surface acceleration for the ground motions imposed on (a) AHA01 and (b) AHA02 (Afacan et al. 2013).

Nonlinear site response simulations were performed using DeepSoil and OpenSees, and equivalent linear simulations were performed using DeepSoil. Ground motions recorded from an accelerometer embedded in the clay near the base of the centrifuge modeling container were imposed as "within" motions following

the guidance of Kwok et al. (2007). The motion of the base plate was not used in these simulations because slip between the base plate and latex membrane containing the soil was observed during shaking.

The site response modeling focuses on two fundamental issues: (1) proper modeling of shear strength, and (2) correction of shear strength to account for strain rate effects. Each of these topics is discussed in detail, and we then present seven different models that utilize different combinations of modeling approach (nonlinear vs. equivalent linear, OpenSees vs. DeepSoil), and shear strength. Comparisons between predicted and measured ground motions are presented in the form of residuals of spectral accelerations versus period, and Arias intensity and cumulative absolute velocity versus peak base acceleration.

1.1 Adjusting Modulus Reduction Curve to Provide Desired Shear Strength

Modulus reduction curves are commonly derived from cyclic laboratory tests that extend to strain amplitudes as high as about 0.3%. Many combinations of earthquake ground motions and soil conditions will result in peak strains that are lower than 0.3%, in which case analyses can be performed within the range of experimental validation of the modulus reduction curves. However, strong ground motions imposed at the base of soft soil layers may result in shear strains that exceed 0.3%, possibly mobilizing shear failure in extreme conditions. This is precisely the scenario for which nonlinear site response analysis is anticipated to provide the largest benefit relative to equivalent linear methods. However, such analyses require extrapolation beyond the range of experimental validation. Often, the equations defining the modulus reduction curves at small strains are simply extrapolated to large strains. This procedure can result in significant under-prediction or over-prediction of shear strength depending on the ratio of shear strength to small strain shear modulus.

To demonstrate this issue, the Darendeli (2001) modulus reduction curve equation (Eq. 1) is defined for the bay mud using a=1.05, and $\gamma_{ref}=(0.035+0.001\cdot PI\cdot OCR^{0.25})\cdot(\sigma_o')^{0.5}$. The value of G_{max} was obtained from the V_s profile in Fig. 2.

$$\frac{G}{G_{\max}} = \frac{1}{1+\left(\frac{\gamma}{\gamma_r}\right)^a} \tag{1}$$

A stress-strain curve can be computed from a modulus reduction curve as $\tau = G\,\gamma$. A true shear strength, defined as a horizontal asymptote for the stress-strain curve, does not exist for Darendeli's modeling

equation for values of *a* unequal to 1.0. Therefore an implied shear strength τ_{imp} is taken as the value of shear stress corresponding to a shear strain of 10%. The values of τ_{imp} are plotted along with measured monotonic undrained strengths in Fig. 5. Additionally, strain-rate-corrected shear strength profiles, described later in the report, are also shown in Fig. 5. The shear strengths implied by Darendeli's equation are significantly lower than the measured monotonic undrained shear strengths in this case. The fact that Darendeli's equation does not accurately capture shear strength is not surprising considering the equation is valid only up to 0.3%. However, this exercise clearly illustrates that the high strain portion of modulus reduction curves should be altered to obtain a desired shear strength.

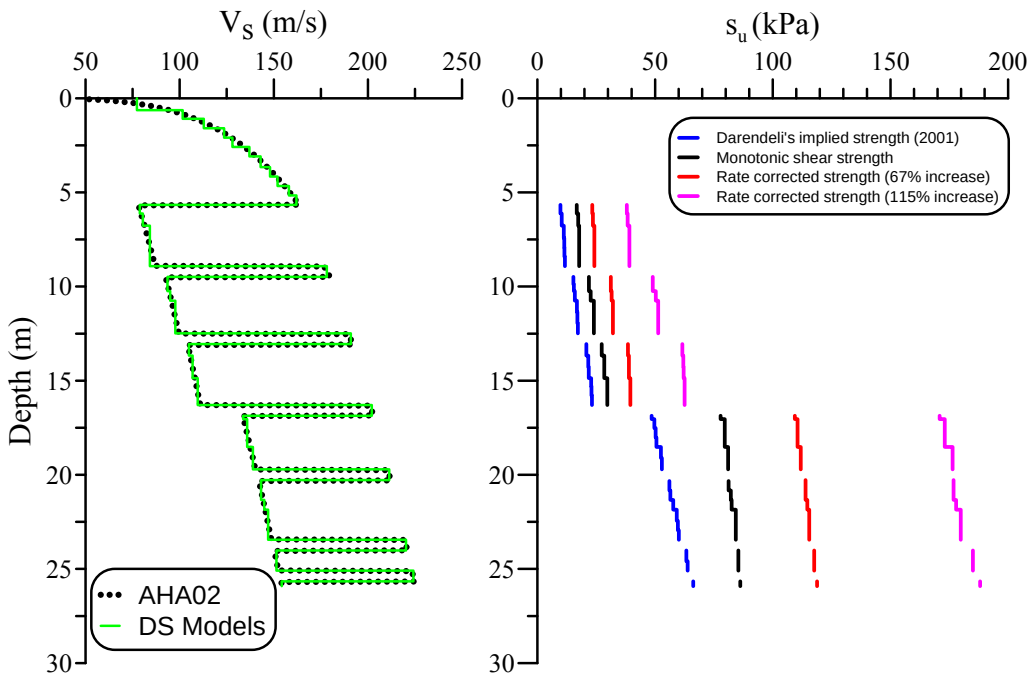

Figure 5. Shear wave velocity profile and shear strength profile.

Yee et al. (2013) developed a procedure that correctly captures a desired shear strength by extrapolating a modulus reduction to high strains using a hyperbolic function that asymptotically approaches the desired shear strength. The procedure involves the following steps: (1) select a transition shear strain, γ_t, at which to transition from the modulus reduction curve to the hyperbolic function, (2) compute the tangent stiffness of the stress strain curve, G_{tan}, at this strain level based on the modulus reduction curve equation (Eq. 2 for Darendeli functional form), (3) compute the shear stress associated with the transition strain, τ_t, (Eq. 3), (4) compute a reference shear strain for the hyperbolic portion of the stress-strain curve (Eq. 4), and (5) compute the stress strain curve using the modulus reduction curve if $\gamma < \gamma_t$ and the

hyperbolic curve if $\gamma \geq \gamma_t$ (Eq. 5). This procedure results in a stress-strain backbone curve that is continuous, and whose slope is continuous, and approaches the desired shear strength.

$$G_{\tan} = \frac{G_{\max}\left[\left(\frac{\gamma_t}{\gamma_r}\right)^a - a\left(\frac{\gamma_t}{\gamma_r}\right)^a + 1\right]}{\left[1+\left(\frac{\gamma}{\gamma_r}\right)^a\right]^2} \tag{2}$$

$$\tau_t = \frac{G_{\max}\cdot\gamma_t}{1+\left(\frac{\gamma_t}{\gamma_r}\right)^a} \tag{3}$$

$$\gamma_{rt} = \frac{s_u - \tau_t}{G_{\tan}} \tag{4}$$

$$\begin{aligned} \tau &= \frac{G_{\max}\cdot\gamma}{1+\left(\frac{\gamma}{\gamma_r}\right)^a} \qquad \textit{if} \quad \gamma < \gamma_t \\ \tau &= \tau_t + \frac{G_{\tan}\cdot(\gamma-\gamma_t)}{1+\left(\frac{\gamma-\gamma_t}{\gamma_{tr}}\right)} \qquad \textit{if} \quad \gamma \geq \gamma_t \end{aligned} \tag{5}$$

An example calculation demonstrating the Yee et al. correction is performed for the upper lift of clay from AHA02 for which PI = 40, OCR = 1.15, σ_o' = 48 kPa, s_u = 17 kPa, and V_s = 80 m/s. Three different values of the transitional shear strain, γ_t, are plotted for reference, along with the extrapolated Darendeli curve. As the value of γ_t increases, the Yee et al. modulus reduction curve more closely resembles the Darendeli curve. Despite very minor differences in the modulus reduction curve at large strains, the stress-strain curves are significantly different, and the Darendeli curve approaches a strength that is less than 60% of the monotonic undrained shear strength, whereas the Yee et al. curves all approach the undrained strength. This is a clear indication that very minor adjustments to the large-strain portion of the modulus reduction curve cause very significant changes in the implied strength, and care must be taken to adjust the tail of the modulus reduction curve to accurately reproduce a target strength.

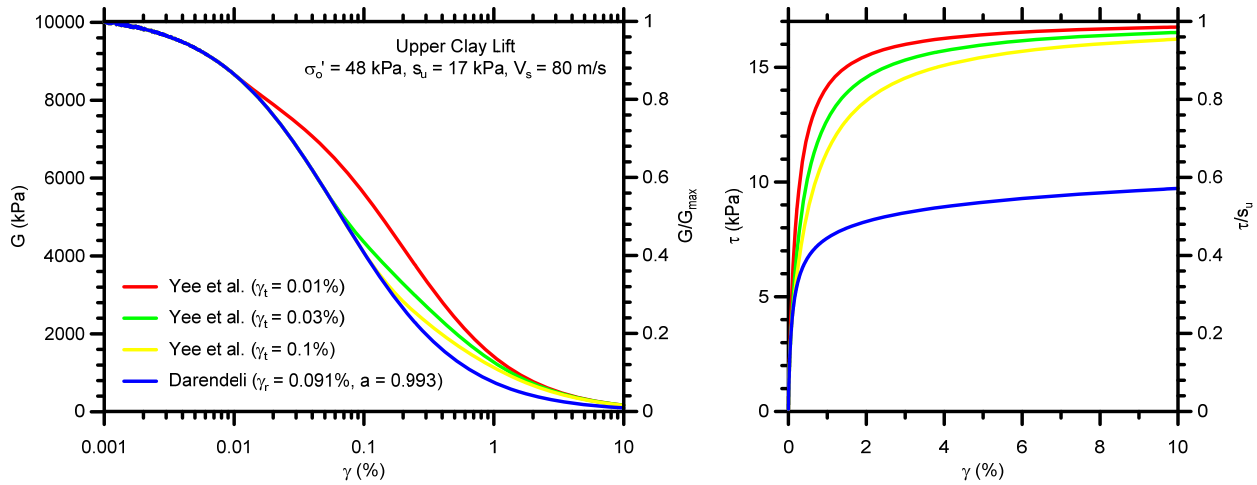

Figure 6- Illustration of Yee et al. (2013) curve-fitting procedure to obtain a desired shear strength.

DeepSoil utilizes a hyperbolic backbone curve that can be curve fit to a target modulus reduction curve using a least-squares regression algorithm. However, the algorithm attempts to fit the entire modulus reduction curve, and very small misfits at large strain can result in significant deviations from the desired shear strength, as demonstrated in Fig. 6. In general, the hyperbolic fit resulted in an under-prediction of the desired shear strength for the clay soils in this study. To solve this problem, we adopted an iterative procedure in which the "target" modulus reduction curve was seeded with erroneously high values at high strain until the resulting stress-strain curve fit the target strength (Hashash, personal communication). This increased the misfit at small strain, but this is a compromise that must be made in the current DeepSoil implementation.

1.1 Correction of Shear Strength for Strain Rate Effects

The shear strength of soil is known to depend upon strain rate. Sheahan et al. (1996) performed laboratory tests on clay specimens and found that the undrained shear strength increased approximately 9% per log cycle increase in strain rate for a range of strain rates from 0.05%/hr to 50%/hr. The centrifuge tests mobilized strain rates as high as 6000%/s, which exceeds the range of the Sheahan et al. study by a factor of 36,000. Yong and Japp (1969) performed tests on clays at much higher strain rates consistent with blast loading, and found that the increase in shear strength is a nonlinear function of strain rate. Strength

increases at a rate consistent with that proposed by Sheahan et al. at rates lower than about 100%/s, whereas shear strength increases more rapidly at rates higher than 100%/s.

Figure 7 shows stress-strain pairs recorded at stress peaks mobilized during the centrifuge test for the upper clay layer in AHA02. The undrained shear strength of the clay measured at a typical laboratory strain rate (assumed to be 20%/hr) is about 17 kPa for this soil. The peak mobilized shear stress is approximately 37 kPa, which is a 115% increase in undrained strength. Backbone stress-strain curves obtained using the Darendeli (2001) modulus reduction curve equation combined with the Yee et al. (2013) procedure are superposed on the data. These backbone curves correspond to the monotonic undrained strength, a strength increase of 67% (consistent with the Sheahan et al. finding), and a strength increase of 115%. The highest curve envelopes the measured data, which we consider to be the most appropriate backbone since the recorded data points should reside within the region bounded by the backbone curve (we do not necessarily anticipate the data points to lie on the backbone curve due to the broadband nature of the input motion and the strain history developed during shaking; a previous cycle may introduce permanent strain in a particular direction prior to the peak stress being recorded).

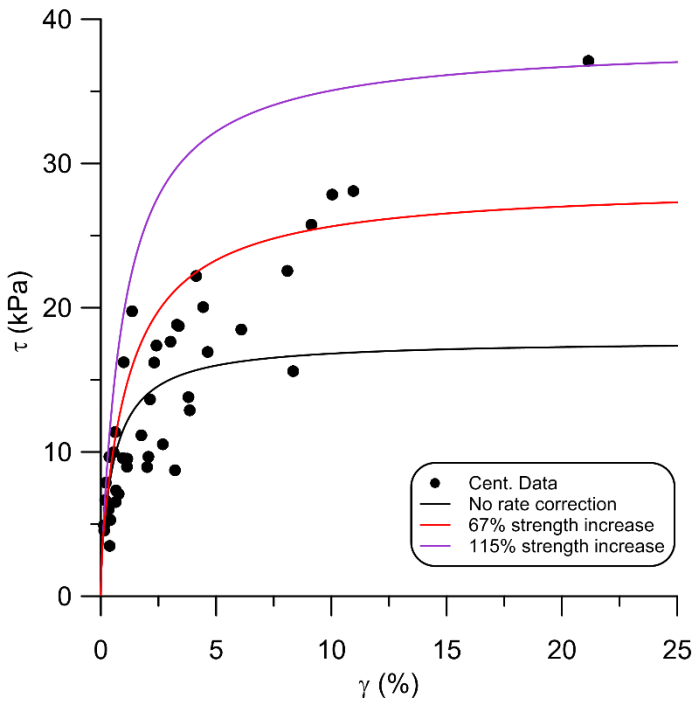

Figure 7- The backbone shear stress curves for the top clay layer. Model 1 uses the modulus reduction and damping curves generated by Darendeli (2001) procedure, Model 2 uses the modulus reduction and damping curves generated by Yee et al. (2013) and Model 3 follows the Yee et al(2013) procedure considering the rate effect

Figure 8 shows the undrained strength ratio versus strain rate including the range of strain rates tested by Sheahan et al. (1996), Yong and Japp (1969), and the peak strain rate measured in the centrifuge test (which also happens to be associated with the peak stress and peak strain measurement). Sheahan et al. and Yong and Japp tested different soils and there was no range of overlap in the strain rates they tested, but the relative increase suggested by Sheahan et al. was similar to that suggested by Yong and Japp for strain rates lower than about 100%/s, after which the strength increase increases more sharply with increase in strain rate. Based on these observations, we have constructed a curve for the bay mud tested in the centrifuge test based on the assumption that the monotonic undrained strength measurement is associated with a strain rate of 20%/hr. The peak measured shear stress lies between the extrapolation of the Sheahan et al. laboratory testing program, and the rapid increase in strength at high strain rate observed by Yong and Japp. More research is required to more fully characterize the strength increase over the full range from typical laboratory strain rates to very high strain rates anticipated during earthquake loading. Although the model scale peak centrifuge strain rate was very high (approx. 6000 %/s), high strain rates would also be anticipated for shear failure under prototype shaking conditions. The prototype strain rate in this case would be about 100 %/s, which is well above the range measured by Sheahan et al. However, the best currently available evidence indicates that the Sheahan et al. extrapolation would be appropriate for the prototype strain rates associated with the centrifuge test, and that this rate correction can be applied for analysis of field cases until better information becomes available through additional research.

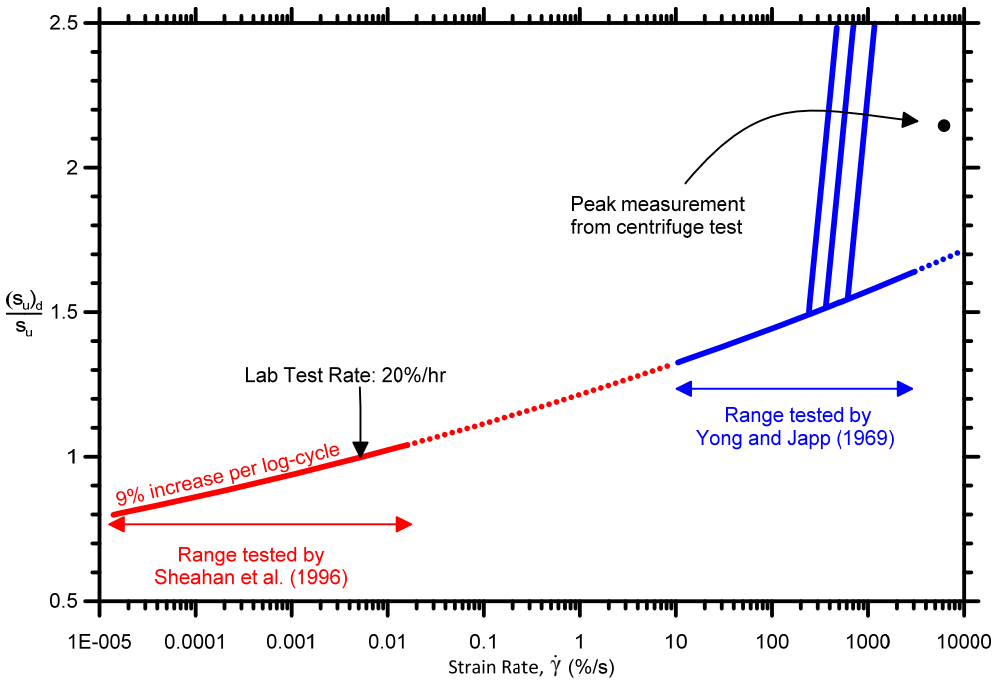

Figure 8- Strain rate effect measured by Sheahan et al. (1996), Yong and Japp (1969), and the peak stress-strain point measured in the centrifuge test.

1.2 Site Response Modeling Analyses

A total of seven different models were performed for various combinations of modeling platforms (DeepSoil and OpenSees), analysis approaches (nonlinear and equivalent linear), and shear strength profiles (Table 1). Undrained shear strength was set to be equal to the strength implied by extrapolating the Darendeli relation (Model 1), the monotonic undrained strength (Model 2), a rate-correction of 115%, which is consistent with the peak measured ratio of $(s_u)_d/s_u$ (Models 3, 4, and 5), and a rate-correction of 67%, which is consistent with the correction by extrapolating Sheahan et al. to high strain rates (Models 6 and 7).

Table 1. Configuration of seven models analyzed in this study.

Model #	Nonlinear (NL) or Equivalent Linear (EQ)?	Modeling Platform	Modulus Reduction Curve	Damping Curve	Shear Strength Correction	Rate Correction
Model 1	NL	DeepSoil	Darendeli (2001)	Darendeli (2001)	None	0%
Model 2	NL	DeepSoil	Darendeli (2001)	Darendeli (2001)	Yee et al. (2013)	0%
Model 3	NL	DeepSoil	Darendeli (2001)	Darendeli (2001)	Yee et al. (2013)	115%
Model 4	NL	OpenSees	Darendeli (2001)	Masing's Rules	Yee et al. (2013)	115%
Model 5	EQ	DeepSoil	Darendeli (2001)	Darendeli (2001)	Yee et al. (2013)	115%
Model 6	EQ	DeepSoil	Darendeli (2001)	Darendeli (2001)	Yee et al. (2013)	67%
Model 7	NL	DeepSoil	Darendeli (2001)	Darendeli (2001)	Yee et al. (2013)	67%

DeepSoil is used for all of the models other than Model 4, which uses OpenSees instead. In DeepSoil, the target modulus reduction and damping curves were obtained using the hyperbolic fitting procedure described previously (the "UIUC" approach in DeepSoil). In OpenSees, the PressureIndependMultiYield (PIMY) material model (Elgamal et al., 2003) was used for the clay layers and the PressureDependMultiYield (PDMY) models as used for the sand layers. The outer yield surface was set to model the desired undrained shear strength, and the intermediate yield surfaces were set to match the desired modulus reduction backbone curve. The PIMY and PDMY material models adopt Masing's rules for unload-reload behavior, which is known to over-predict damping at high strains, as shown in Fig. 9. Kwok et al. (2007) discussed various methods for matching the modulus reduction and damping curves using codes that rely upon Masing's rules. In this report, we match the modulus reduction curve, and accept a misfit in hysteretic damping.

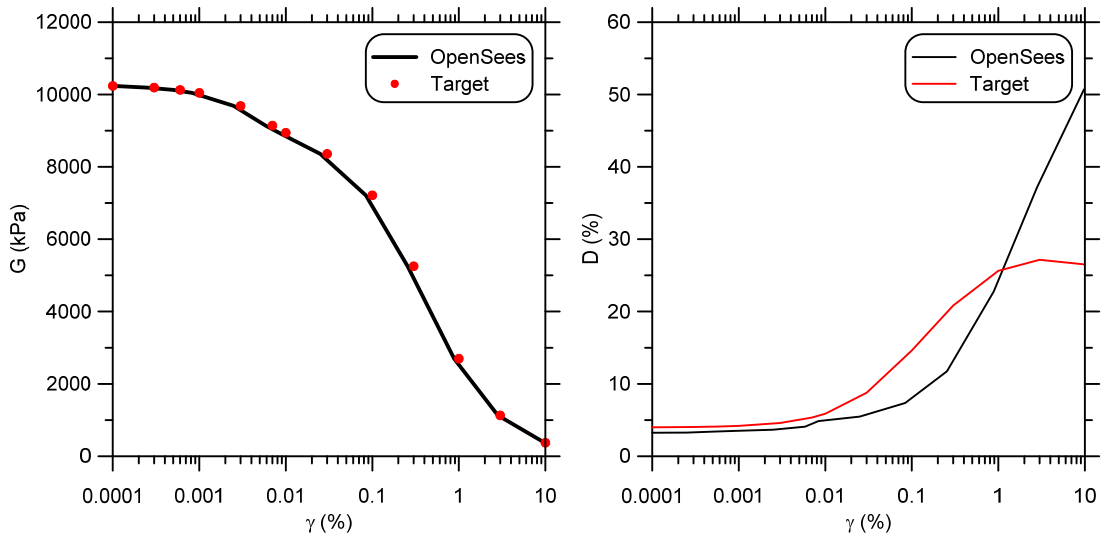

Figure 9 – Shear modulus reduction and damping curves obtained from OpenSees compared to the target.

DeepSoil and OpenSees also have different approaches to modeling small-strain damping. DeepSoil provides an option to use a frequency-independent Rayleigh damping procedure (Hashash and Park 2004), a full Rayleigh damping procedure that permits specification of damping at two frequencies, and a simple Rayleigh damping procedure in which damping is matched at only a single frequency. We utilized the frequency-independent Rayleigh damping procedure despite its added computational cost. However, the frequency-independent algorithm is not implemented in OpenSees, and we therefore utilized full Rayleigh damping instead. The full Rayleigh damping equations are shown below.

$$a_0 = \frac{2.\xi_T.\omega_1.\omega_2}{\omega_1 + \omega_2} \tag{6}$$

$$a_1 = \frac{2.\xi_T}{\omega_1 + \omega_2} \tag{7}$$

$$\xi_R = \frac{a_0}{2.\omega} + \frac{a_1.\omega}{2} \tag{8}$$

where ξ_T is the target damping ratio and ω_1 and ω_2 are the angular frequencies associated with the target damping. The Rayleigh damping curves used in DeepSoil and OpenSees are shown in Figure 10.

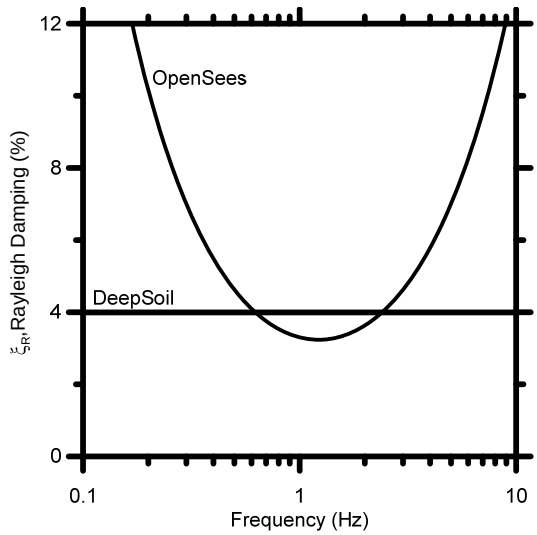

Figure 10 - Rayleigh damping as a function of frequency

The numerical models utilized for the nonlinear site response analysis consist of 50 layers in order to capture the frequency content of the ground motions used in the study. Elements that are too large form a low-pass filter that prevents propagation of short wavelengths. The friction angle for the sand layers was set to 40°, which is reasonably consistent with estimates using Bolton's (1986) procedure, assuming a critical state friction angle of 32° for the Monterey sand.

1.3 Site Response Modeling Results

This section presents results for the site response modeling simulations compared with the test data. We first present computed and recorded time series, acceleration response spectra, and profiles of peak acceleration and peak shear strain for a single ground motion scaled to three different intensities. We then present residuals (defined as measured response minus predicted response) for spectral acceleration and other ground motion intensity measures.

1.3.1 Influence of Undrained Shear Strength

Time series and response spectra (5% damping) for three scaled versions of the WPI046-1994 Northridge Earthquake recording are shown in Fig. 11. Measured data from AHA02 are compared with computed results from Models 1, 2, and 3. Models 1 and 2 consistently under-predict the surface motion, with the prediction error increasing as shaking intensity increases. Model 3 properly considers strain rate effects on undrained shear strength, whereas Models 1 and 2 use significantly smaller shear strengths. Profiles

of peak acceleration and mobilized shear strain are shown in Fig. 12. The larger motions produced peak shear strains in the soft clay on the order of 4% to 8%, which is essentially large enough to mobilize the strength of the clay. The lower strengths associated with Models 1 and 2 limited the transmission of ground motion, thereby resulting in an under-prediction of surface motion. On the other hand, Model 3 properly modeled the undrained strength by including strain rate effects, and correctly predicted the ground motion. The smaller motion mobilized shear strains on the order of 0.4% in the soft clay, which is too small to mobilize the undrained strength. However, this strain level is large enough that the shear strength has an influence on the stress-strain behavior, as illustrate by the Yee et al. procedure in Fig. 6. Note that the mobilized shear strain (0.4%) is significantly higher than the transition shear strain (0.05%) applied using the Yee et al. procedure. An interesting observation is that none of the models predicted shear strains in the soft clay as high as the measured shear strain for the two larger motions, yet the ground motion predictions are reasonably consistent. A possible reason for this observation is that the shear strain levels mobilized in the simulations were still high enough to mobilize the undrained strength of the clay (e.g., 3 to 4% for the largest motion), and the ground acceleration is being limited by failure of the clay.

Two conclusions are drawn from the comparisons in Figs. 11 and 12: (1) modeling shear strength correctly is important for predicting ground motion using nonlinear site response analysis, even if shear strains are not high enough to mobilize the shear strength, and (2) strain rate significantly influences undrained shear strength in clay and should be included in site response simulations to avoid under-predicting ground motion.

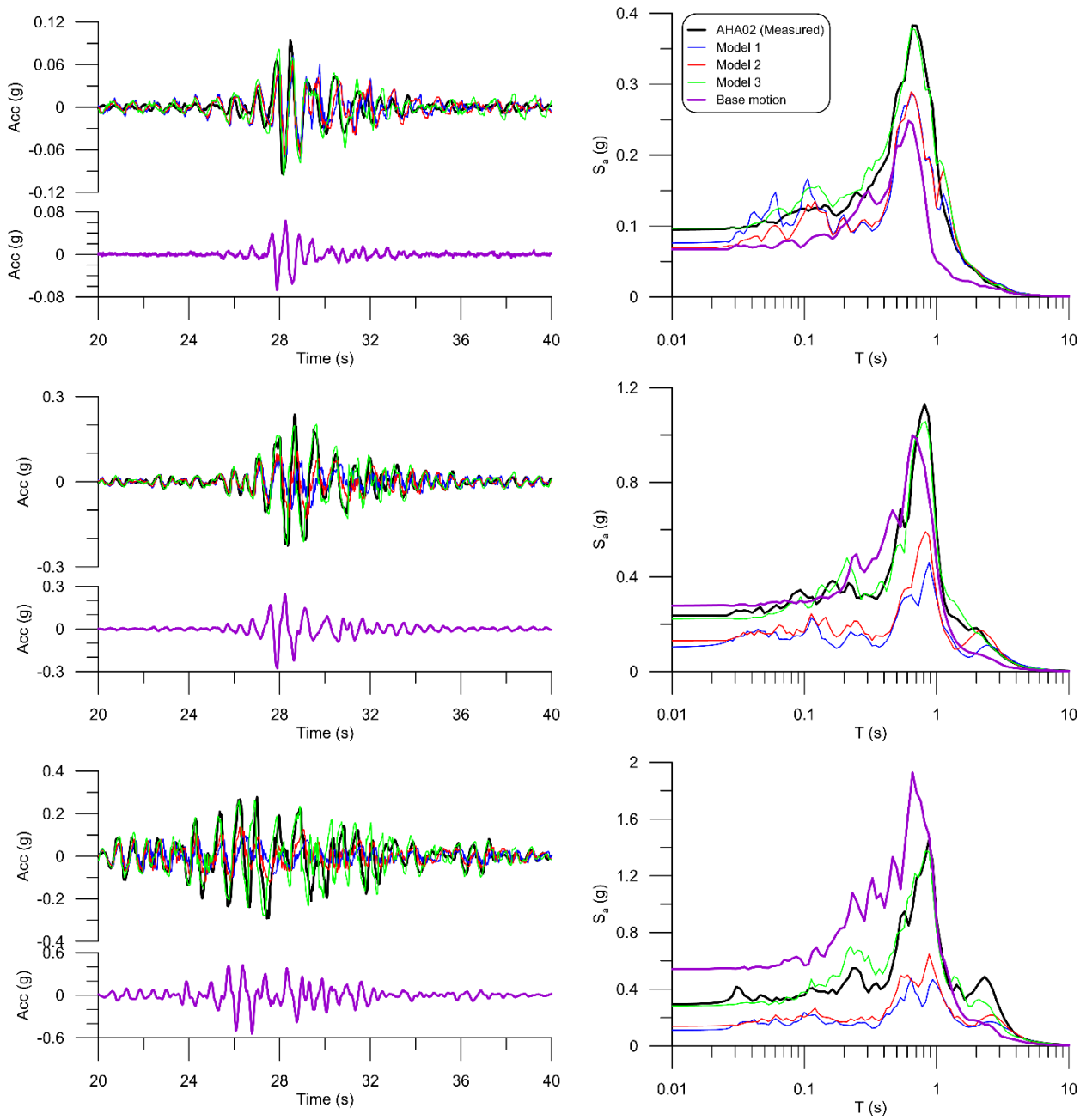

Figure 11 - Example acceleration time series and spectral accelerations of surface motions for the centrifuge data and the nonlinear simulations

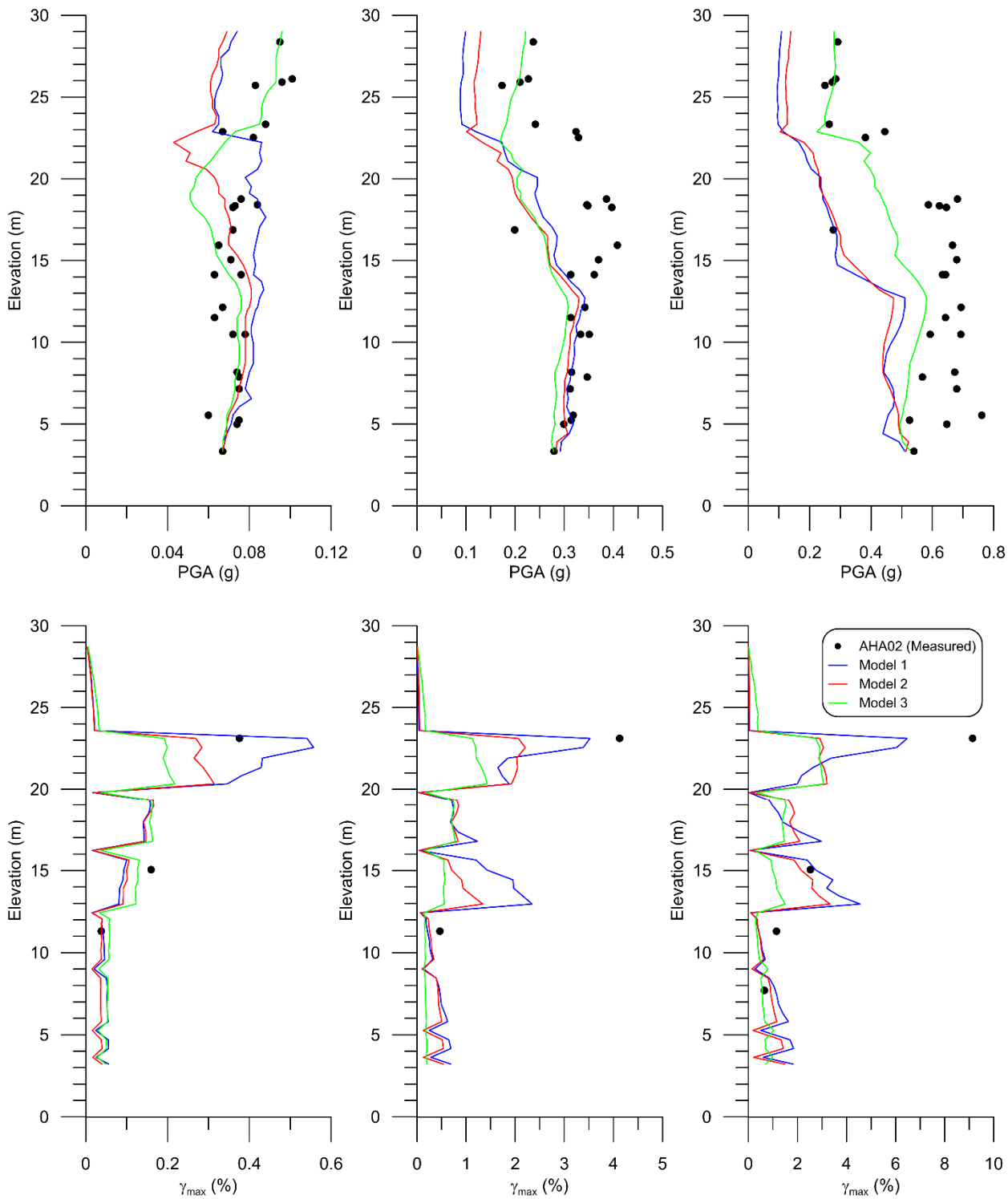

Figure 12- Peak horizontal acceleration and the maximum shear strain profiles for Model 1,2 and 3.

1.3.2 Comparison of DeepSoil and OpenSees

The same three ground motions are compared in Figs. 13 and 14 using DeepSoil and OpenSees simulation platforms (Models 3 and 4). The results are very similar for all three motions, which indicates that differences between the simulation platforms do not significantly influence the outcome for this particular problem. The primary difference between the two analysis procedures is the hysteretic and small-strain Rayleigh damping formulations. DeepSoil is able to more accurately capture both sources of damping than the models implemented in OpenSees. In particular, we anticipated over-damping at high strain in the OpenSees model due to the Masing rule damping formulation. However, the strain levels mobilized in the OpenSees simulations are only on the order of 3% to 4%, which are associated with only modest differences between the target damping curve and the one achieved in OpenSees, and the differences may be offset by under-prediction of damping at smaller strains (see Fig. 9).

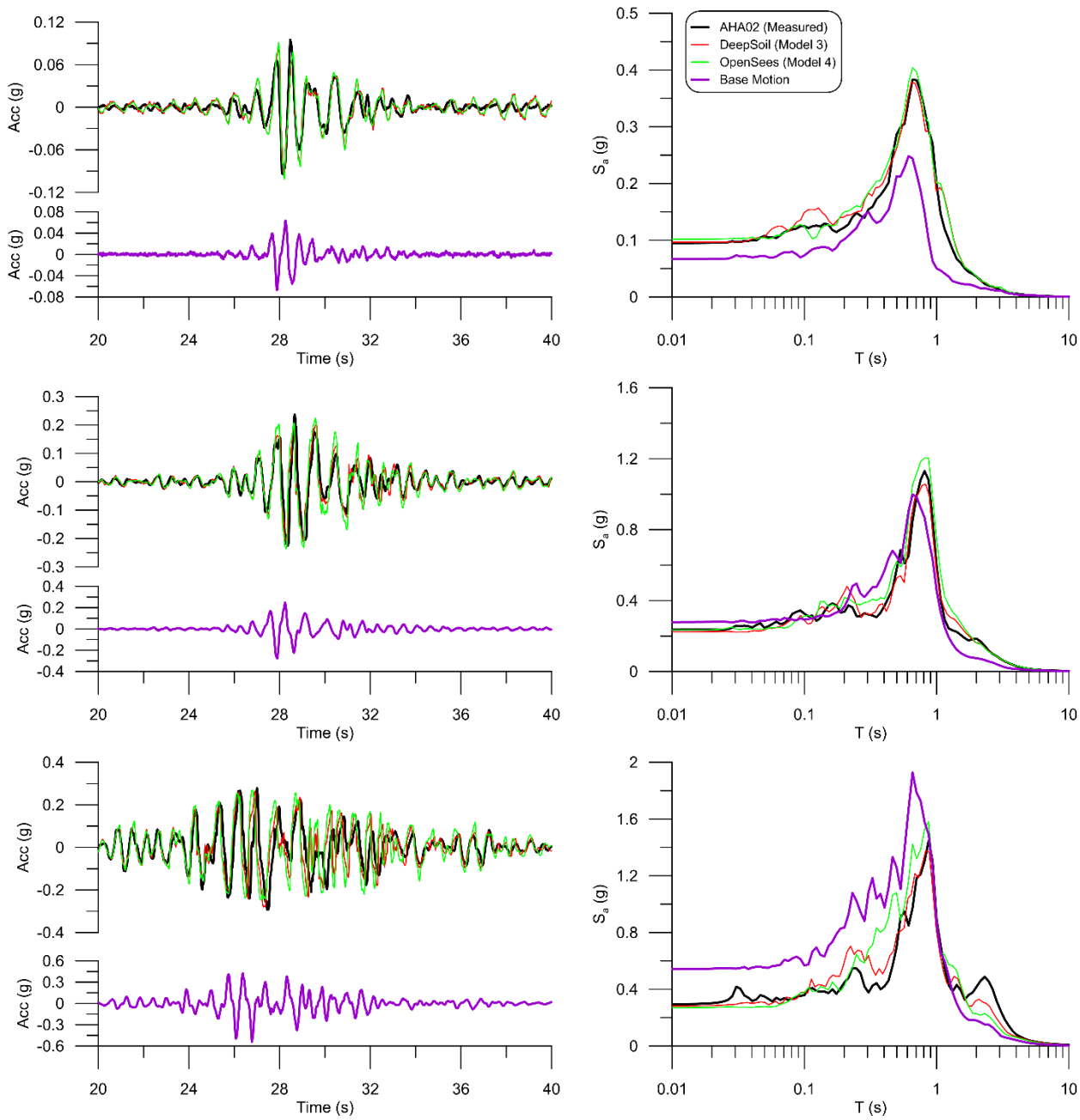

Figure 73 - Example acceleration time series and spectral accelerations of surface motions for the centrifuge data and the nonlinear simulations using DeepSoil (Model 3) and OpenSees (Model 4).

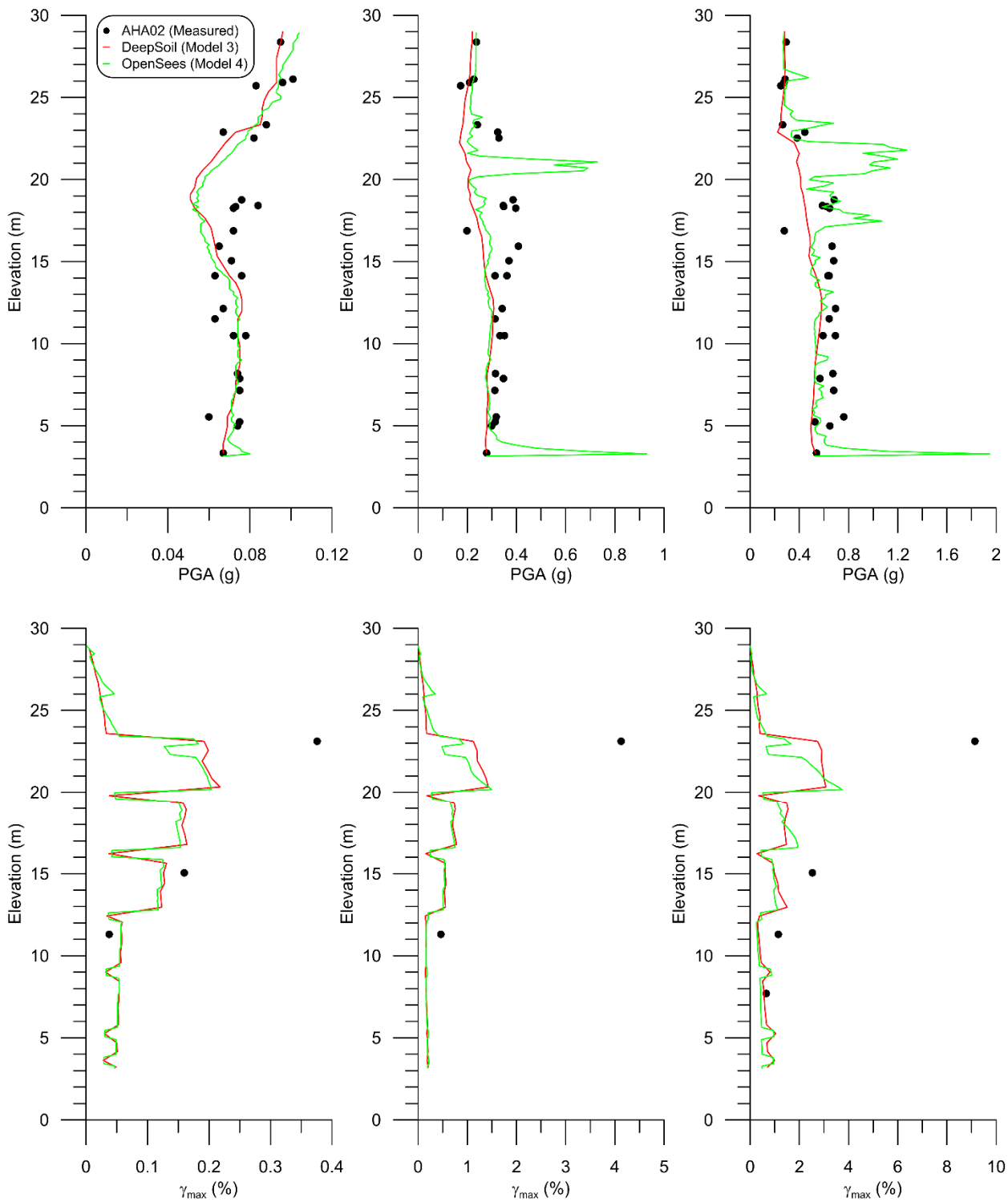

Figure 84 - Peak horizontal acceleration and the maximum shear strain profiles for Model 3 and 4.

1.3.3 Comparison of Nonlinear and Equivalent Linear Simulations

A comparison between nonlinear (Model 3) and equivalent linear (Model 5) site response simulations, both following a modulus reduction curve with a 115% increase in shear strength for rate effects, are shown in Figs. 15 and 16. The equivalent linear simulation agrees very well with the nonlinear simulation for the small motion, as anticipated since the largest differences are anticipated for larger motions and associated larger shear strains. The equivalent linear simulation tends to over-predict ground motion for the larger two motions. Interestingly, the equivalent linear simulation predicts larger strains than the nonlinear simulation in the softest clay layer. Errors in the equivalent linear approach are also readily apparent for the small cycles that precede the large cycles during the ground motion, as illustrated in Fig. 17. The phase and amplitude in this portion of the equivalent linear record do not match the measurements nearly as well as the nonlinear site response simulation. This observation is caused by the equivalent linear assumption that the secant shear modulus is constant for the entire record, whereas in reality it varies in time because strain amplitude varies in time. These errors in the equivalent linear site response simulations are subsequently demonstrated to cause errors in ground motion intensity measures that integrate ground motion in time (i.e., Arias intensity and cumulative absolute velocity).

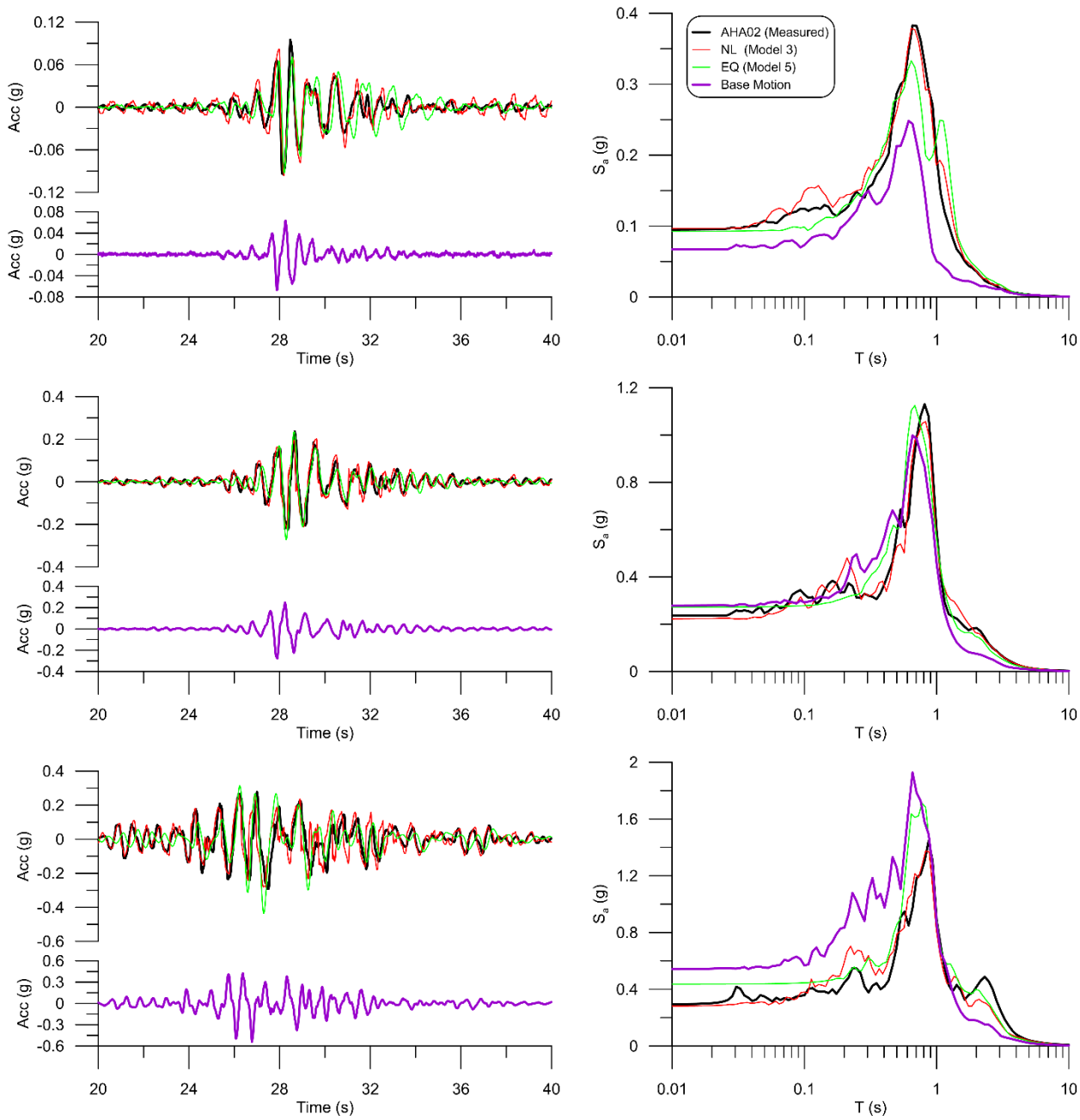

Figure 95 - Example acceleration time series and spectral accelerations of surface motions for the centrifuge data and the nonlinear (Model 3) and equivalent linear (Model 5) simulations.

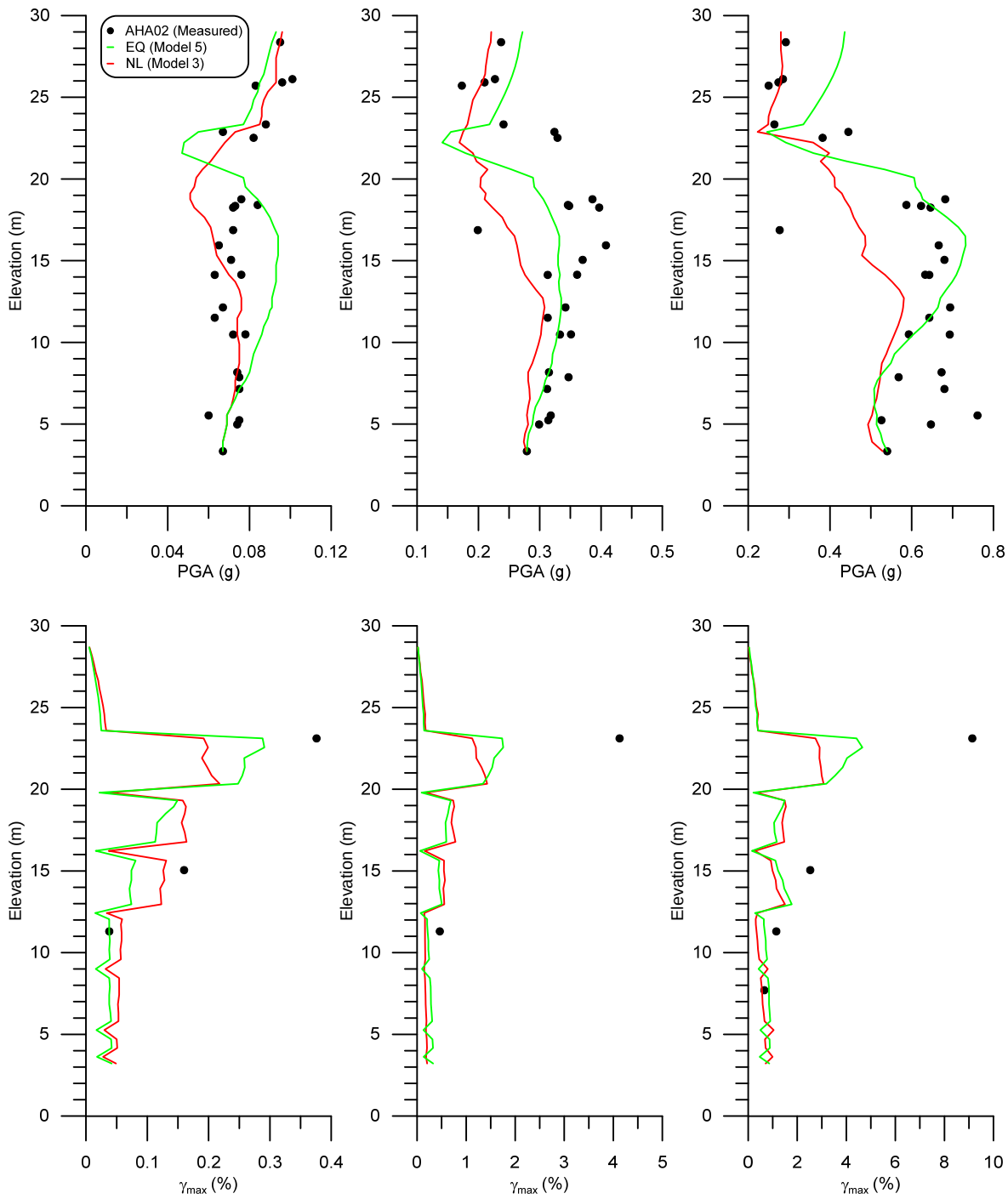

Figure 106 - Peak horizontal acceleration and the maximum shear strain profiles for Models 3 and 5.

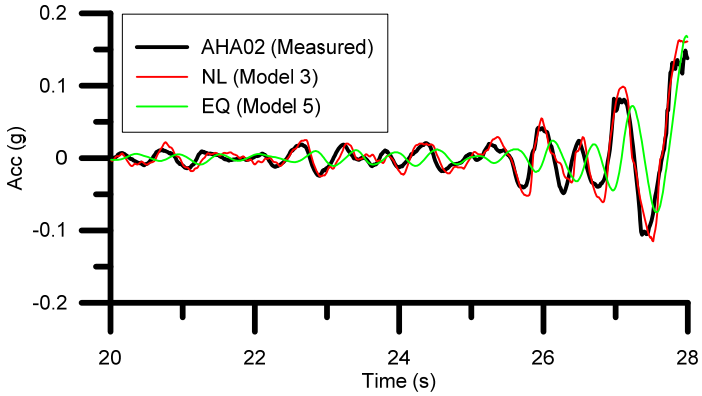

Figure 117 – Zoomed-in view of the medium amplitude motion from Fig. 15 showing the amplitude and phase errors in the small portion of motion for the equivalent-linear analysis.

1.3.4 Influence of strain rate correction

The influence of strain rate correction is shown in Figs. 18 and 19 for Models 6 and 7, which utilize a 67% increase in strength following the Sheahan et al. (1996) finding rather than the measured 115% increase in strength. Decreasing the shear strength results in an under-prediction of ground motion for the nonlinear analysis (Model 7) and a slight reduction for the equivalent linear analysis (Model 6). The fact that Model 6 is actually improved by utilizing the incorrect shear strength is an indication that counterbalancing errors are in effect here. These figures indicate that obtaining the correct undrained strength is very important, and further illustrates that more work is needed to fully quantify rate effects over the full range of rates anticipated in site response studies.

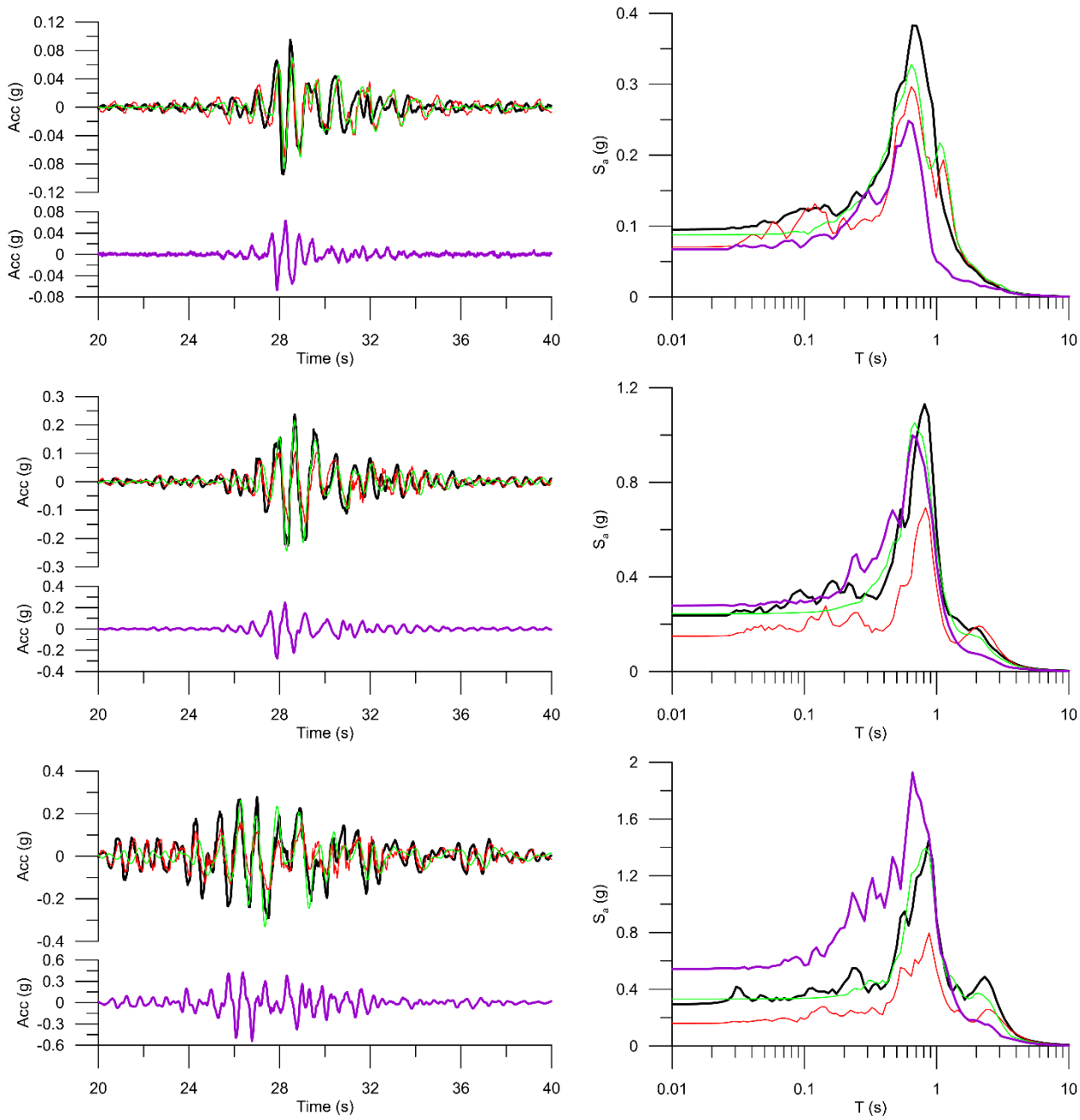

Figure 128 - Example acceleration time series and spectral accelerations of surface motions for the centrifuge data and the nonlinear (Model 7) and equivalent linear (Model 3) simulations using a 67% increase in strength rather than the measured 115% increase in strength.

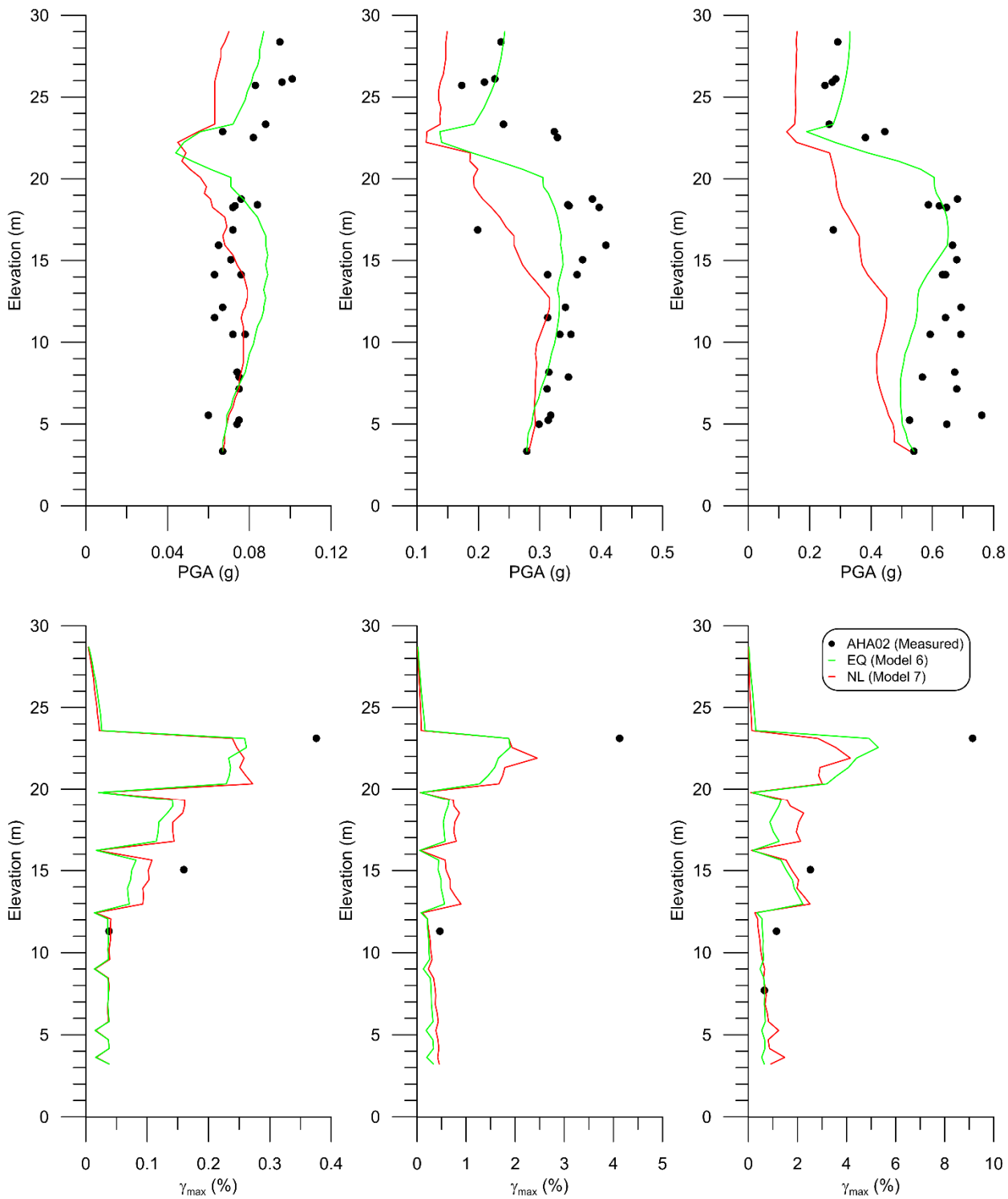

Figure 139 - Peak horizontal acceleration and the maximum shear strain profiles for Models 6 and 7.

1.3.5 Residuals of Various Ground Motion Intensity Measures

Residuals of various ground motion intensity measures are presented in this section to demonstrate the overall accuracy of each site response modeling approach. Acceleration response spectra (5% damping) for the surface motion were computed for a period range from 0.01 to 10s, and residuals were computed by taking the difference in the natural log of spectral acceleration between the measurement and the prediction. A positive residual indicates an under-prediction of ground motion. The residuals are plotted with different symbols for small motions (peak base acceleration, PBA < 0.1g) and medium and large motions (PBA > 0.1g). The most accurate of all of the procedures is Model 3, which is the DeepSoil nonlinear site response analysis that uses the correct undrained shear strength. Second is the OpenSees nonlinear site response analysis that also uses the correct undrained shear strength. The third most accurate is Model 6, which is an equivalent linear analysis in DeepSoil using an undrained shear strength that is too low because the rate correction is only 67% rather than 115%. However, this model shows a general negative bias in the residuals, particularly at short period. The other models show significant bias, particularly for the medium and large motions. Differences among the models largely pertain to shear strength, so it makes sense that an erroneous assumption about shear strength will result in the most bias for large motions.

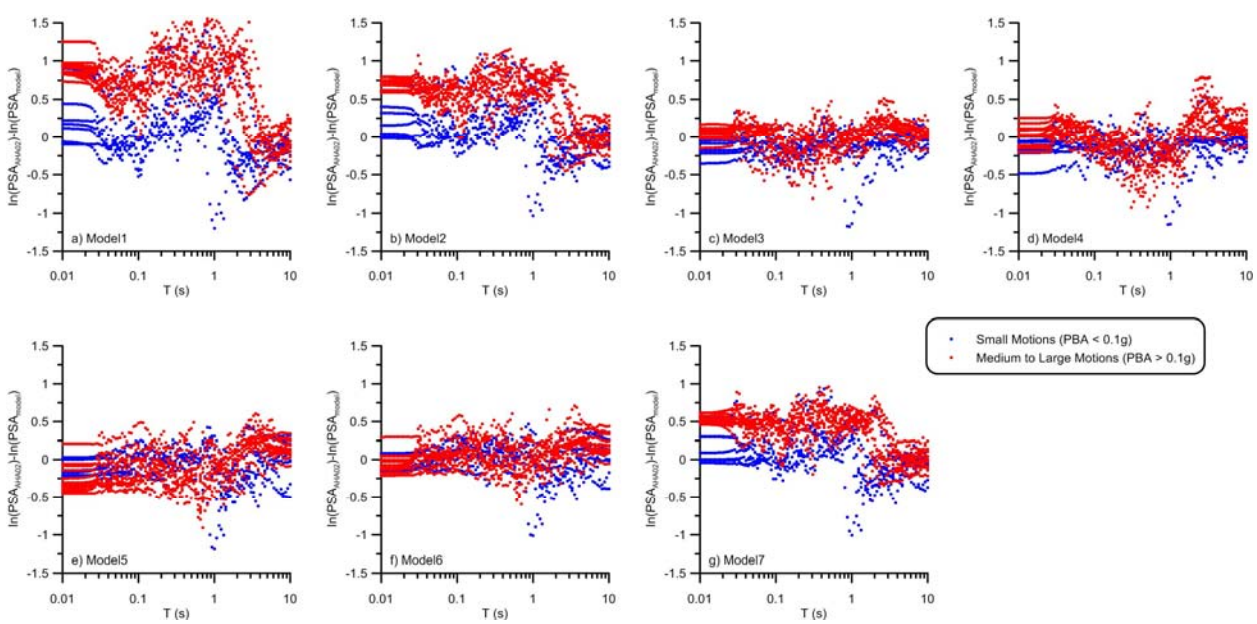

Figure 20 – Residuals (measurement minus prediction) of the natural logarithm of spectral acceleration versus spectral period.

Residuals were also computed for Arias intensity and cumulative absolute velocity, as shown in Figs. 21 and 22. For both intensity measures, Models 3 and 4 again tend to be more accurate than the other

models. However, more bias is apparent, as is a slight trend with PBA for small motions. The other models all exhibit significant trends in the residuals with PBA, indicating that they are likely to produce large errors in predictions of Arias intensity and cumulative absolute velocity. This may be an important finding since these intensity measures are increasingly being used to predict damage of earth structures such as earth dams.

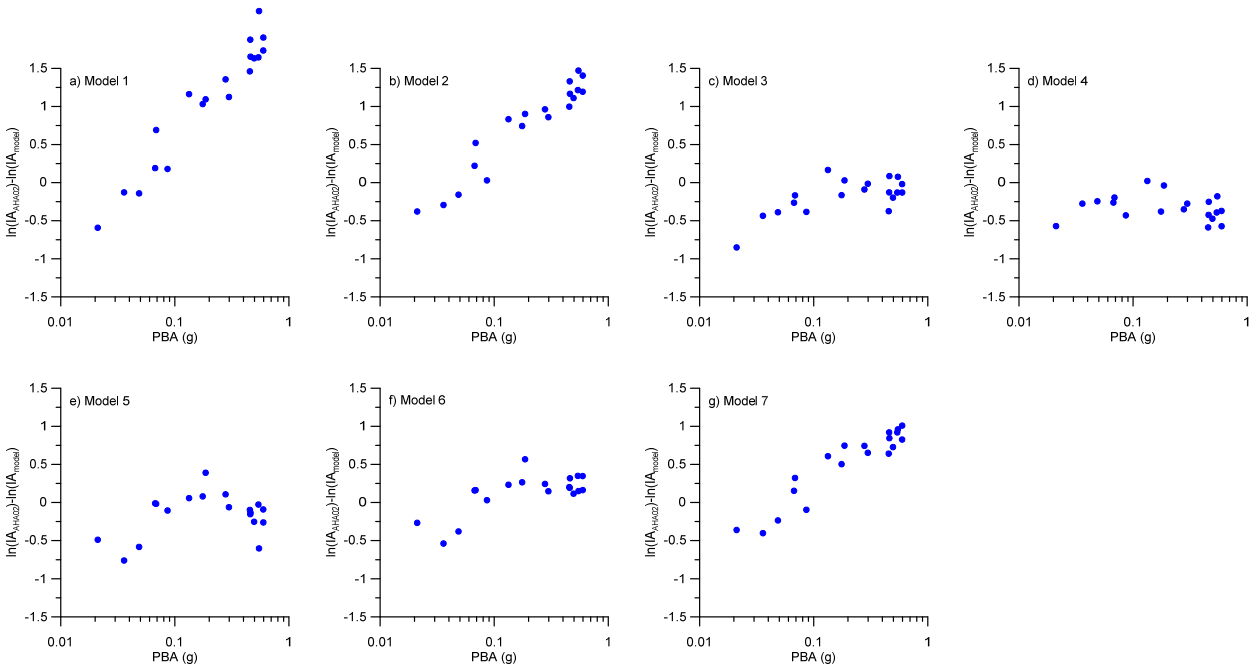

Figure 21 – Residuals of Arias intensity (IA) versus peak base acceleration.

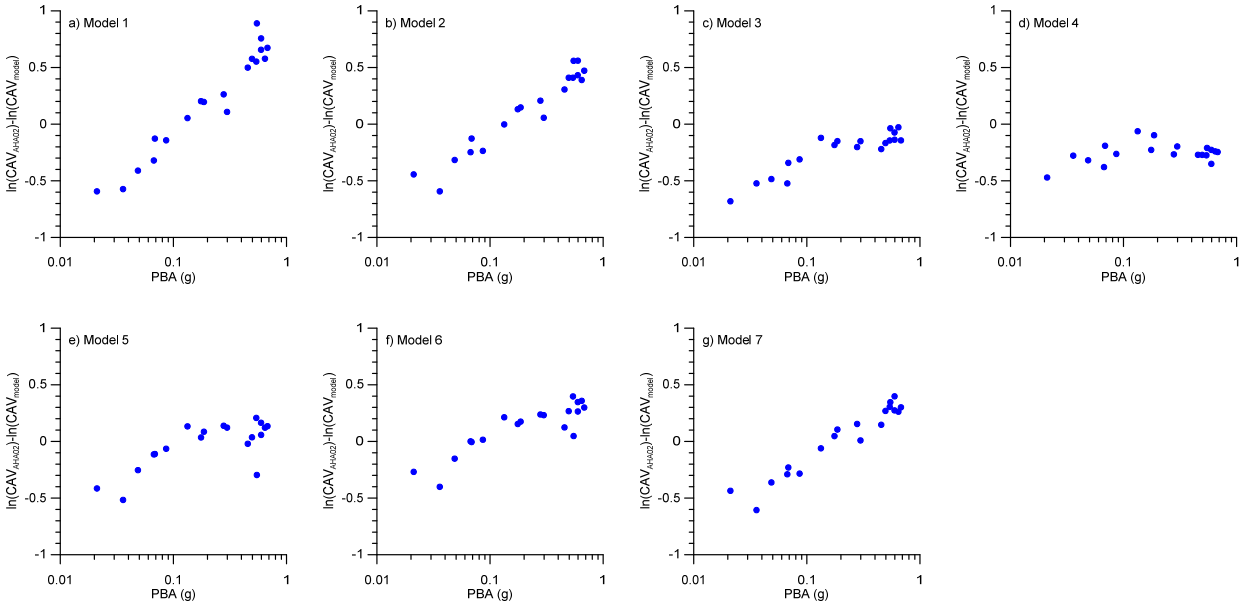

Figure 142 – Residuals of cumulative absolute velocity (CAV) versus peak base acceleration.

2 Effective Stress Nonlinear Site Response Analysis of Centrifuge Models Involving Liquefaction

Liquefaction of cohesionless soils is widely acknowledged to exert an influence on earthquake ground motions. However, significant disagreements exist regarding the extent to which liquefaction attenuates or amplifies ground motion. A common argument made by many researchers is that liquefaction provides a "base isolator" effect that prevents propagation of vertical shear waves, thereby protecting overlying soil layers and sometimes preventing liquefaction of these layers (e.g., Martin and Qiu 2001). The "base isolator" effect, however, does not agree with observations of high frequency and sometimes high amplitude acceleration pulses that propagate through liquefied soil. Such observations have been made in strong motion records in the field, in physical modeling studies, and in numerical simulations that utilize constitutive models that properly capture dilatancy. In this chapter we seek to demonstrate that the "base isolator" effect is an erroneous outcome of a simplifying assumption made in the modeling of pore pressure generation in certain types of effective stress site response codes, and we show that proper treatment of dilatancy using advanced constitutive models can capture the high frequency high amplitude acceleration pulses.

2.1 Measurement of Acceleration Pulses in Liquefied Sand

Perhaps the most well-known recording of ground motion and pore pressure during earthquake-induced liquefaction is the Wildlife Liquefaction Array recordings from the 1987 Superstition Hills earthquake. Acceleration and pore pressure recordings clearly documented liquefaction at the site. Figure 23 shows the north-south acceleration recorded at the surface and 5.7m deep, and a pore pressure measurement in the liquefiable material (Holzer and Youd, 2007). The acceleration amplitude and frequency content tend to decrease with the buildup of significant excess pore pressure, with the exception of several high-frequency, moderate amplitude acceleration spikes late in the record. For example, a high-frequency 0.1g spike is apparent in the surface acceleration measurement at about time = 54s, which corresponds to a similarly sharp drop in the pore pressure record. This response occurred after development of significant pore pressures, and clearly demonstrates that liquefied sand is not a soft, weak base isolator and that at least moderate ground shaking can propagate through liquefiable soil.

Evidence of this phenomenon is also provided by the NIG018 N/S record in Kashiwazaki from the 2007 Niigata Ken Chuetsu-Oki earthquake (Kayen et al. 2007) shown in Fig. 24. The strong motion station rests on an alluvial sand deposit with SPT blow counts around 20 at depths of about 5 to 9m (just below the water table) and denser materials at depth. The peak surface acceleration recorded at the site was 0.7g, producing estimated CSR>0.4, and placing the sand clearly on the "liquefaction" side of the Seed and Idriss (1971) simplified procedure (or any other triggering procedure for that matter). Surface evidence of liquefaction was found at sites very near the recording station.

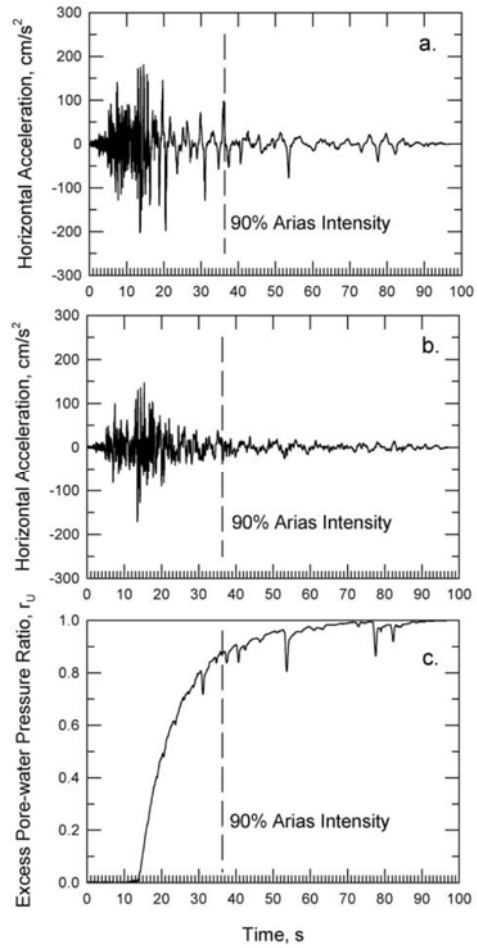

Figure 153. Wildlife liquefaction data recorded during 1989 Superstition Hills Earthquake (Holzer and Youd 2007).

Figure 24 shows the acceleration records and acceleration response spectra for two ground motion records both obtained on the surface projection of the fault plane (R_{jb} = 0). The primary difference in these records is the site conditions; the NIG018 site was susceptible to liquefaction whereas the 65039 site was not. The NIG018 acceleration record clearly shows large-amplitude acceleration spikes. Unlike the Wildlife site, where the high-frequency acceleration spikes were smaller than the peak horizontal acceleration, the peak horizontal acceleration in this case occurred during one such spike and is directly attributed to the undrained response of soil during cyclic loading. Hence, the high-frequency spikes are not merely an interesting academic artifact of liquefied soil behavior, but rather control the peak ground motions. To demonstrate this point further, the 65039 ground motion on non-liquefied ground was significantly lower. The 65039 station response spectrum has a fairly typical shape with a pronounced peak at about 0.3s, whereas the NIG018 response spectrum contains a very broad band over which spectral accelerations are high, and does not exhibit the characteristic low-period peak. The broad band in the NIG018 spectrum can be explained by the impulse-like acceleration pulses. Impulses exhibit a flat frequency response, and would therefore be expected to cause a broad band acceleration response spectrum. The difference between the 65039 and NIG018 records may be partially attributed to path effects or site effects that are unrelated to liquefaction, but the dilatant behavior of sand in undrained loading site response clearly played a role in the observed motions at the NIG018 site, and the liquefied sand clearly did not act as a

"base isolator". In fact, the NIG018 station recorded the largest peak horizontal acceleration and velocity of any K-net station during the earthquake.

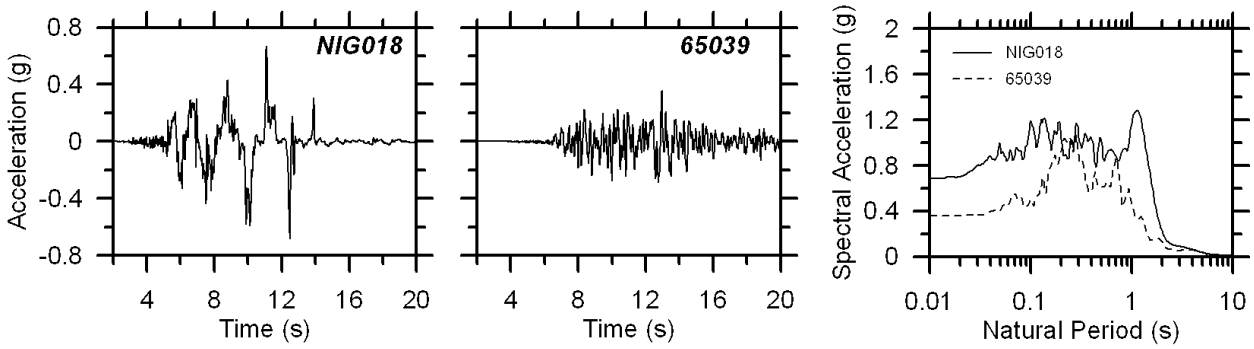

Figure 164. Ground motions from a site that liquefied (NIG018) and did not liquefy (65039) during 2007 Niigata Ken Chuetsu Oki earthquake. Both recording stations were on the surface projection of the fault plane (R_{jb} = 0).

A final example of this behavior from a centrifuge test is shown in Figure 25, where peak accelerations of more than 1g were observed during strong shaking, and were clearly related to the recorded drops in pore pressure (Brandenberg et al., 2005). The acceleration amplitude was large enough to cause the capacitive accelerometer to "clip", meaning that its capacity was exceeded and it exhibited a capacitive decay in voltage. The acceleration pulses correspond to transient reductions in pore pressure ratio, which is similar to the Wildlife Liquefaction Array response, though the acceleration pulses and transient pore pressure reductions are more pronounced.

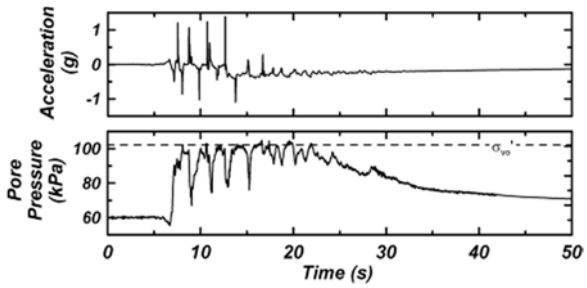

Figure 175. Acceleration and pore pressure record in liquefied sand from centrifuge test (Brandenberg 2005).

2.2 Explanation of Acceleration Pulses in Liquefied Sand

The presence of large-amplitude high-frequency spikes of acceleration in ground motions from liquefiable sites may seem surprising based on the assumption that liquefied sand is very weak, but is not surprising

considering the well-known influence of dilatancy on undrained stress-strain behavior of sands. Fig. 26 shows a stress-controlled cyclic triaxial test on Sacramento River sand conducted by Boulanger and Truman (1996). The sand gradually softens and eventually reaches a state of zero effective stress, i.e., $p'/p_c'=0$, at which point the sand does indeed exhibit a very low shear modulus. However, the liquefied sand does not remain soft and weak after reaching this state. Rather, the stress-strain response exhibits a strain-hardening behavior in which the tangent shear modulus increases as strain increases, exhibiting an inverted S-shaped stress-strain behavior that has been observed in many other cyclic undrained tests on sands and non-plastic silts. The stress path follows the critical state line in q-p' space, forming the characteristic butterfly shape. The strain-hardening behavior is caused by the dilatant tendency of the sand being suppressed in undrained loading.

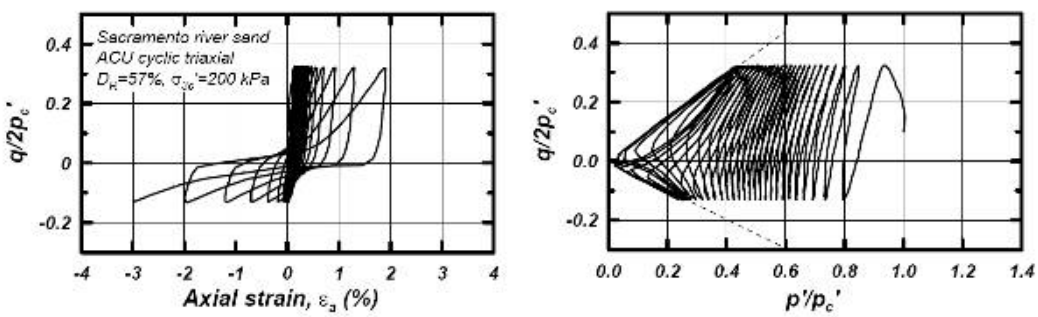

Figure 18.Cyclic triaxial test on saturated Sacramento River sand (Boulanger and Truman 1996).

The sudden increase in effective stress due to dilatancy results in an increase in shear modulus, which enables propagation of wave energy through the soil. This wave energy results in increased shear strains in overlying layers, and a high frequency high amplitude pulse of acceleration propagates through the sand. These waves have been called de-liquefaction shock waves by Kutter and Wilson (1999). Dilatancy of liquefied sand is clearly important for modeling the high frequency acceleration pulses. However, dilatancy is not modeled in some effective stress site response models that are currently used to predict ground motions in liquefying soil profiles. We now turn our attention to explaining modeling assumptions made in various classes of nonlinear effective stress site response models.

2.3 Pore Pressure Generation Models

Early pore pressure generation models proposed by Seed et al (1975) and Booker et al (1976) provided empirical relationship between excess pore pressure ratio, r_u (excess pore pressure normalized by initial confining stress), and number of loading cycles, N. The equation is shown below

$$r_u = \frac{2}{\pi} sin^{-1}\left[\left(\frac{N}{N_{liq}}\right)^{\frac{1}{2\theta}}\right] \tag{9}$$

where r_u is defined as:

$$r_u = \frac{u_x}{\sigma'_{co}} \tag{10}$$

θ is a calibration parameter and N_{liq} is the number of cycles required to initial liquefaction. Both parameters can be determined from stress controlled cyclic triaxial tests. The calibration parameter is dependent on test conditions and the soil type whereas N_{liq} is related to loading intensity and relative density. This equation is intended to capture the low-frequency increase in excess pore pressure ratio, and neglects the transient cycling of excess pore pressure that accompanies undrained laboratory testing.

Matasovic (1992) suggested a functional form for pore pressure generation that is based on accumulation of strain above the volumetric threshold shear strain:

$$r_u = \frac{p.f.F.N_c.\left(\gamma_{ct} - \gamma_{tvp}\right)^s}{1 + f.F.N_c.\left(\gamma_{ct} - \gamma_{tvp}\right)^s} \tag{11}$$

In Eq. 11, p, F and s are the curve fitting parameters and f is the parameter that represents the directional pore pressure generation. f is 1 for 1-D condition and 2 for 2-D conditions. The threshold shear strain for initiation of volumetric strain, γ_{tvp}, is between 0.01% to 0.02% and there is no significant pore pressure generation expected for shear strains below this threshold. For soil at the Wildlife Liquefaction Array, the curve fitting parameters were found as p=1.04, F=2.6 and s=1.7.

The excess pore pressure generations results in a reduction of soil strength and the reduction is represented by degradation index, δ_t, where v=3.5-5.0 and it is 3.8 for Santa Monica beach sand.

$$\tau^* = \tau_0.\delta_t = \tau_0.\left[\left(1 - u_N\right)^v\right] \tag{12}$$

An example strain controlled simulation using the Matasovic pore pressure generation model is shown in Fig. 27. A cyclic shear strain with amplitude of 0.05% is imposed on the model, and the pore pressure generation function is computed using Eq. 11. The updated stress amplitude for each cycle was computed using Eq. 12, and the stress-strain loops were generated accordingly. Note that the excess pore pressure ratio increases monotonically during loading, which is consistent with the modeling assumption. In reality, transient oscillations would be present in the pore pressure response due to dilatancy of the sand.

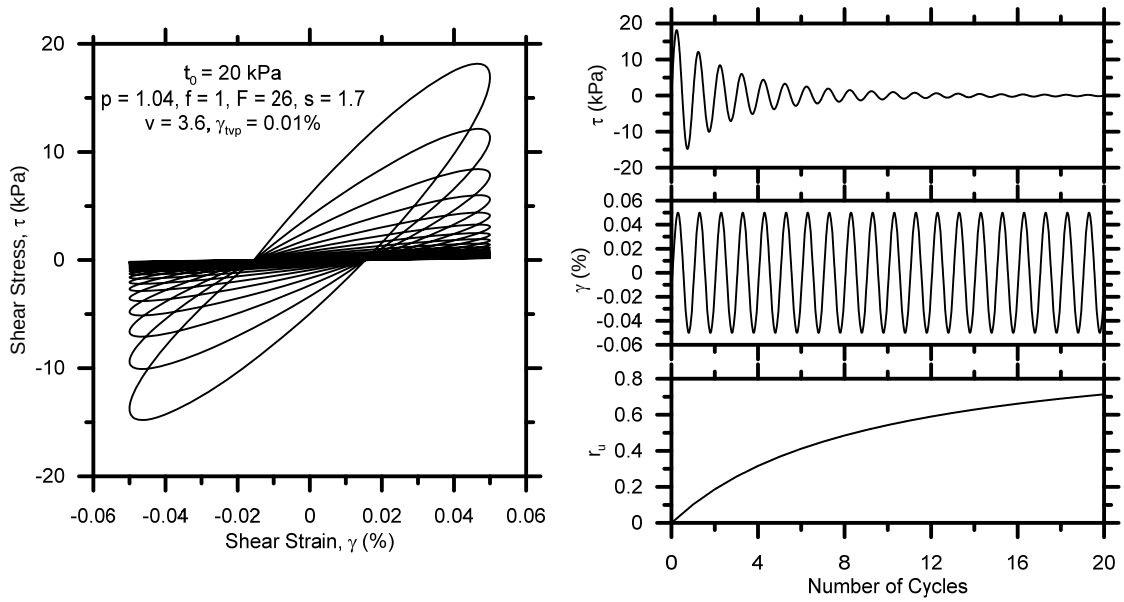

Figure 27. Numerical simulation of undrained strain-controlled test using pore pressure generation function by Matasovic (1992).

Pore pressure generation models have also been formulated based on the hysteretic energy dissipated per unit volume of soil. Dissipated hysteretic energy normalized by initial confining pressure, W_s, was used by Green et al (2000) to develop the following pore pressure generation model:

$$r_u = \sqrt{\frac{W_s}{PEC}} \tag{13}$$

where W_s is

$$W_s = \frac{1}{2\sigma_0^{'}} \sum_{i=1}^{n-1} \left(\tau_{i+1} + \tau_i\right)\left(\gamma_{i+1} - \gamma_i\right) \tag{14}$$

PEC is a calibration parameter that represents the "pseudo energy capacity" and can be determined from cyclic tests. It was empirically derived as:

$$PEC = \frac{W_{s,r_u=0.65}}{0.4225} \tag{15}$$

In 2008, Polito et al modified the calibration parameter and expressed it as follows:

$$In(PEC) = \left\{ \exp(c_3 Dr) + c_4 \right\} \quad \text{for FC<35\%} \tag{16a}$$

$$In(PEC) = \left\{ c_1 FC^{c_2} + \exp(c_3 Dr) + c_4 \right\} \quad \text{for FC≥35\%} \tag{16b}$$

The energy-based pore pressure generation modeling approach is similar to the strain-based modeling approach in that the excess pore pressure ratio increases monotonically and never oscillates due to dilatancy. A fundamental difference between the strain-based and energy-based approaches is that the strain-based approach permits pore pressure generation only when the strain amplitude exceeds the volumetric threshold shear strain, γ_{tvp}. Soil dissipates hysteretic energy at strains lower than γ_{tvp}, yet pore pressure has not been observed to develop at such low strains.

2.4 Advanced Constitutive Models

A thorough review of advanced constitutive models is beyond the scope of this report, and we focus on the ability of the models to capture dilatancy, which bears particular importance for undrained site response analysis in liquefied soils. Different approaches to modeling this behavior include multiple yield surface models (e.g., Elgamal et al. 2003) in which the tangent stiffness is controlled by nested yield surfaces that translate and rotate in stress space, and bounding surface models (e.g., Dafalias and Manzari 2004, Boulanger and Ziotopolou 2012) in which tangent modulus is a function of the distance between the current stress point and a bounding surface. Both modeling approaches can capture the strain-stiffening behavior that is associated with dilatancy of the sand being suppressed during undrained loading, as shown in Figs. 28 and 29. This behavior has been measured during many stress-controlled cyclic laboratory tests. It is not always apparent in constant-amplitude strain-controlled cyclic laboratory tests because the dilatant tendency occurs when the shear strain exceeds the maximum past shear strain, which never happens during constant-amplitude strain controlled tests. Earthquake ground motions

generate a complex loading path that is neither stress-controlled nor strain-controlled, and it is therefore important that stress-strain models are able to capture the dilatant tendency.

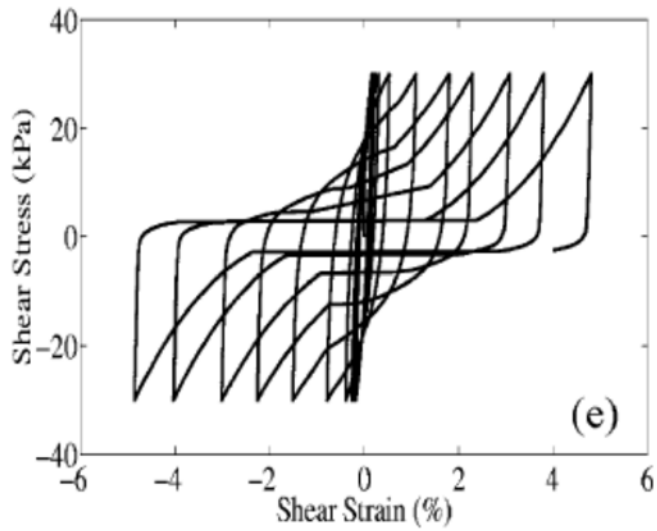

Figure 28. Multiple yield surface plasticity model undrained stress-strain behavior (Elgamal et al. 2003).

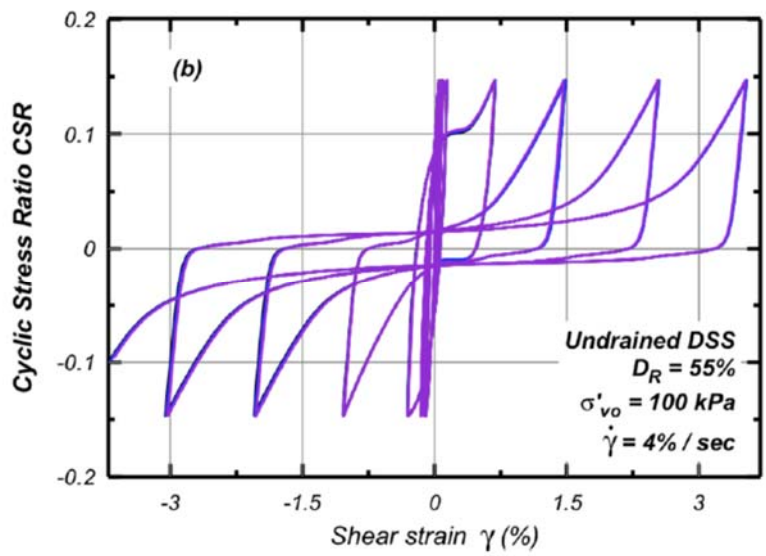

Figure 29. Bounding surface plasticity model undrained stress-strain behavior (Boulanger and Ziotopolou 2012).

2.5 Description of Centrifuge Model CSP3

A centrifuge modeling program presented by Wilson et al. (2000) is utilized in this report to compare the different effective stress modeling approaches. Model CSP3 (Figs. 30 and 31) consists of a medium dense layer of sand (D_R = 55%) overlying dense sand (D_R = 85%) with the groundwater table at the surface. The model was constructed in a shear beam container consisting of steel and aluminum rings separated by flexible rubber layers. A variety of deep foundations were installed in the model, but we focus our attention on a "free-field" array of sensors that are far enough from any of the foundations to minimize interaction effects between the deep foundations and the soil. The model was shaken by a sequence of ground motions, and the large input motions liquefied the medium dense sand layer. We focus our attention in this manuscript on the large ground motions that liquefied the soil to observe the ability of nonlinear effective stress site response codes to (1) capture the buildup of pore pressure and liquefaction triggering, and (2) model the post-liquefaction acceleration pulses associated with dilatancy of the sand.

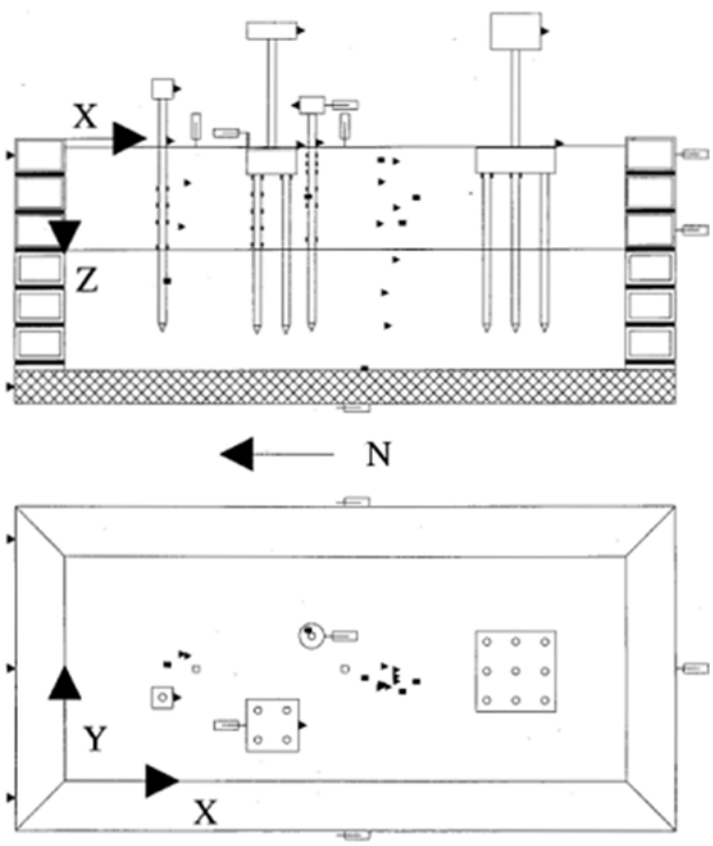

Figure 30. Configuration of model CSP3 (Wilson et al. 2000).

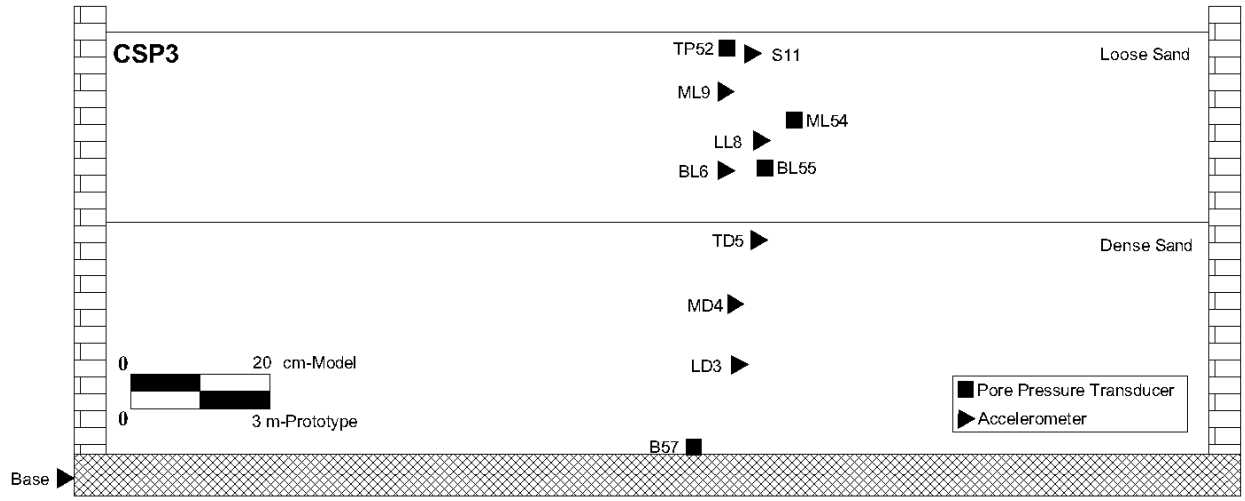

Figure 31. Sensors from CSP3 utilized in this study (pile foundations omitted for clarity).

Unfortunately, a shear wave velocity profile was not measured for the centrifuge tests. However, local experience with Nevada sand indicates that the shear wave velocity profile can be defined using the functional form:

$$V_s = V_{s1}\left(\frac{p'}{p_a}\right)^n \tag{17}$$

where p_a is atmospheric pressure, V_{s1} = 250 m/s for medium dense sand and 280 m/s for dense sand, and n=0.5. Furthermore, we assume K_o=0.5 for defining the mean effective stress profile.

2.6 Site Response Modeling

Four different site response modeling approaches were used to analyze the centrifuge test data, as summarized in Table 2. Models 8, 9, ad 10 are performed in DeepSoil whereas OpenSees is used for Model 11. The Seed and Idriss modulus reduction and damping curves were used to model the dynamic properties of the sand. The friction angle for the medium dense layers was assumed 35° and it was assumed 40° for dense layers. The target strength for each of the 50 layers in the site response models was achieved using the Yee et al. (2013) procedure previously explained in the total stress analysis section. For the DeepSoil nonlinear site response models, the "target" modulus reduction curve was seeded with erroneous values at high strain to obtain a least squares hyperbolic curve fit that provides the desired

shear strength, as described previously in this report. For all of the models, unit weights were 19.5 kN/m^3 for the medium dense layer and 20.0 kN/m^3 for the dense layer.

Table 2. Properties of models for effective stress analysis

Model #	Nonlinear (NL) or Equivalent Linear (EQ)?	Modeling Platform	Modulus Reduction Curve	Damping Curve	Pore Pressure Generation Model or Constitutive Model
Model 8	EQ	DeepSoil	Seed and Idriss, 1991	Seed and Idriss, 1991	N/A
Model 9	NL	DeepSoil	Seed and Idriss, 1991	Seed and Idriss, 1991	Matasovic (1992)
Model 10	NL	DeepSoil	Seed and Idriss, 1991	Seed and Idriss, 1991	Green et al. (2000)
Model 11	NL	OpenSees	Seed and Idriss, 1991	Masing's Rules	Elgamal et al. (2003)

The DeepSoil nonlinear site response models require additional parameters to define pore pressure generation and the rate of shear modulus reduction, and the OpenSees model requires additional constitutive modeling parameters. Model 9 follows the Matasovic approach using curve fitting parameters, p=1.1, F=2.6, and s = 1.7. The volumetric threshold shear strain was set to 0.02% and v is assumed 3.8 for the model based on results presented for Santa Monica beach sand by Matasovic. Model 10 uses the procedure by Green et al. (2000) assuming D_r=55% for the medium dense layers and D_r=85% for the dense layers. The fines content was assumed 0. Model 11 uses the PressureDependMultiYield model and simulations were performed using Cyclic 1-D, a user interface developed specifically for nonlinear effective stress site response. Input parameters for the two different layers are summarized in Table 3.

Table 3. Model parameters for Model 11.

Model parameters	Medium Dense	Dense
Depth Range (m)	0-8.4	8.4-19.2
Reference Shear Wave Velocity, V_{s1} (m/s)[a]	235	250
Reference Confining Pressure, p_r (kPa)	100	100
Confinement Dependence Coefficient, n	0.5	0.5
Lateral Earth Pressure Coefficient, K_o	0.5	0.5
Friction Angle, ϕ' (deg)	35	40
Cohesion, c (kPa)	0	0
Peak Shear Strain (%)	10	10
Number of Yield Surfaces	20	20
Dilat2	4.5	5
liquefac1	0	0
Dilation Angle, ψ (deg)	27	27
Contraction Parameter 1	0.03	0.03
Contraction Parameter 2	0.6	0.6
Dilation Parameter 1	0.75	0.8
Dilation Parameter 2	4.5	5
Liquefaction Parameter 1	0	0
Permeability Coefficient (m/s)	0.0001	0.0001

a) $V_s = V_{s1}\left(\frac{p'}{p_r'}\right)^n$

2.7 Comparison of Site Response Simulations with Measured Results

Acceleration records at four different depths in the model are presented in Fig. 32, along with acceleration response spectra for the motions recorded at these elevations. Pore pressure records are shown in Fig. 33 at several depths where measurements were obtained in the centrifuge tests. Turning first to the acceleration response, at a depth of 15.3 m all of the model predictions agree reasonably well with the measured acceleration records because this recording is fairly close to the base of the model container, and the ground motion does not differ significantly from the base motion. As depth becomes shallower, the model predictions begin to diverge from each other and from the measured ground motion. At a depth of 0.5m (the shallowest recorded ground motion), the recorded motion exhibits a sharp pulse at approximately t = 10s. This acceleration pulse is reproduced in the OpenSees simulation, but not in the other simulation procedures. Shortly after this acceleration pulse, the excess pore pressure ratio reached approximately 1.0 (see Fig. 33) indicating liquefaction occurred in the medium dense layer. Following

liquefaction, a number of additional acceleration pulses are present in the record, and these pulses are associated with transient reductions in the excess pore pressure ratio. These pulses are also captured by the OpenSees simulation, but not the other simulations. Both pore pressure generation models predict significantly lower ground motion than what was measured following liquefaction triggering. In fact, the equivalent linear simulation predicts more accurate post-liquefaction ground motion amplitude than the pore pressure generation models, although the frequency content of the equivalent linear ground motion does not agree with measurements.

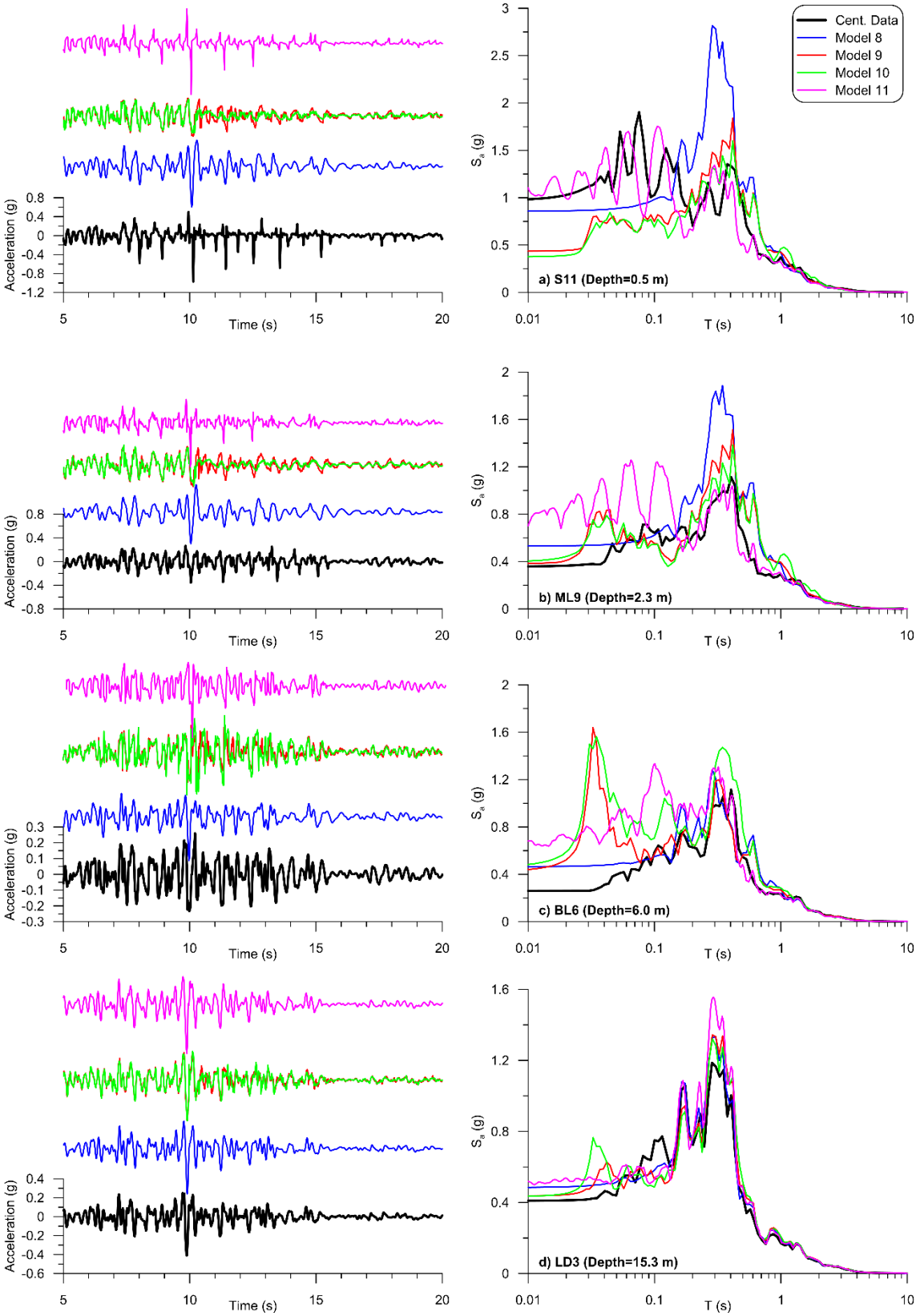

Figure 32. Ground motion predictions at various depths using four different modeling approaches.

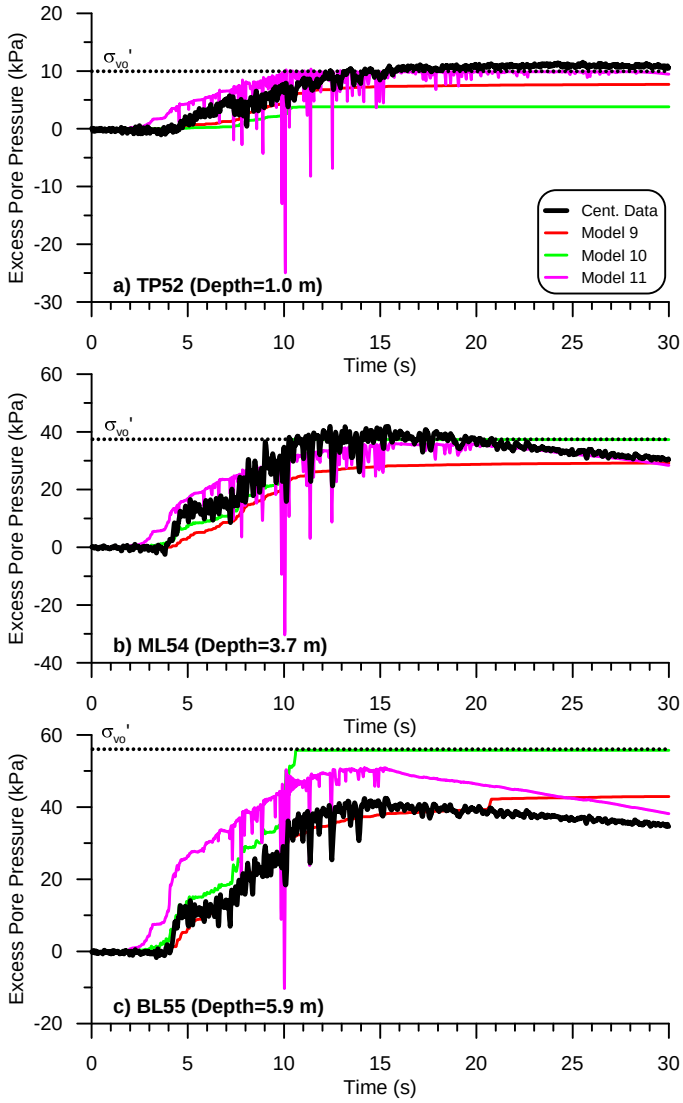

Figure 33. Measured and predicted pore pressure responses.

Turning to the pore pressure responses, the centrifuge model reached a condition of full liquefaction at depths of 1.0m and 3.7m, but did not approach full liquefaction at 5.9m. The Model 9 simulation predicted that none of the layers would fully liquefy (i.e., reach a condition of zero effective stress), whereas the Model 10 simulation predicted full liquefaction at depths of 5.9m and 3.7m, but not at 1.0m. The OpenSees simulation (Model 11) predicted full liquefaction at depths of 1.0m and 3.7m, but not at 5.9m, which agrees well with measurements. The Model 10 simulation illustrates a base isolator effect, in which full liquefaction deep in the profile reduces propagation of earthquake ground motion at shallower depths, thereby shielding these shallow layers from liquefying. On the other hand, significant motion did propagate through the soil profile and the near-surface layers did liquefy. Also note that Model 9 and 10

predict a monotonically increasing excess pore pressure ratio, whereas the measurements and Model 11 predict transient oscillations in which excess pore pressure ratio decreases. Model 11 is therefore more accurate than Models 9 and 10 in this regard.

Profiles of peak acceleration and peak shear strain are shown in Fig. 34. Model 10 exhibits a concentration of high shear strain at a depth of approximately 4m, where full liquefaction is predicted for this model. A similar concentration of strain occurs at a depth of 3m for Model 9, although this model did not fully liquefy. The concentration of strain in a particular layer can be easily explained by the modeling assumption that pore pressure can only increase, but never decrease, using a pore pressure generation model. As pore pressures begin to increase in the element with the highest shear strain demand, the soil softens and accumulates more strain thereby generating even more pore pressure. This process continues until this element has fully liquefied. After liquefaction, very little ground motion propagates through the liquefied zone since this element is so soft forming what has been called a "base isolator" effect, which explains why the shear strains are smaller at depths shallower than the critical element. However, this "base isolator" effect is not observed in the measured data. The peak measured acceleration was nearly 1.0g at a depth of 0.5m, compared with predicted accelerations of only about 0.4g using the pore pressure generation models. By contrast, the OpenSees model predicts the acceleration at this depth reasonably well. The OpenSees model over-predicts accelerations deeper within the model, which could be related to modeling errors, or non-one-dimensional wave propagation due to container effects in the centrifuge model.

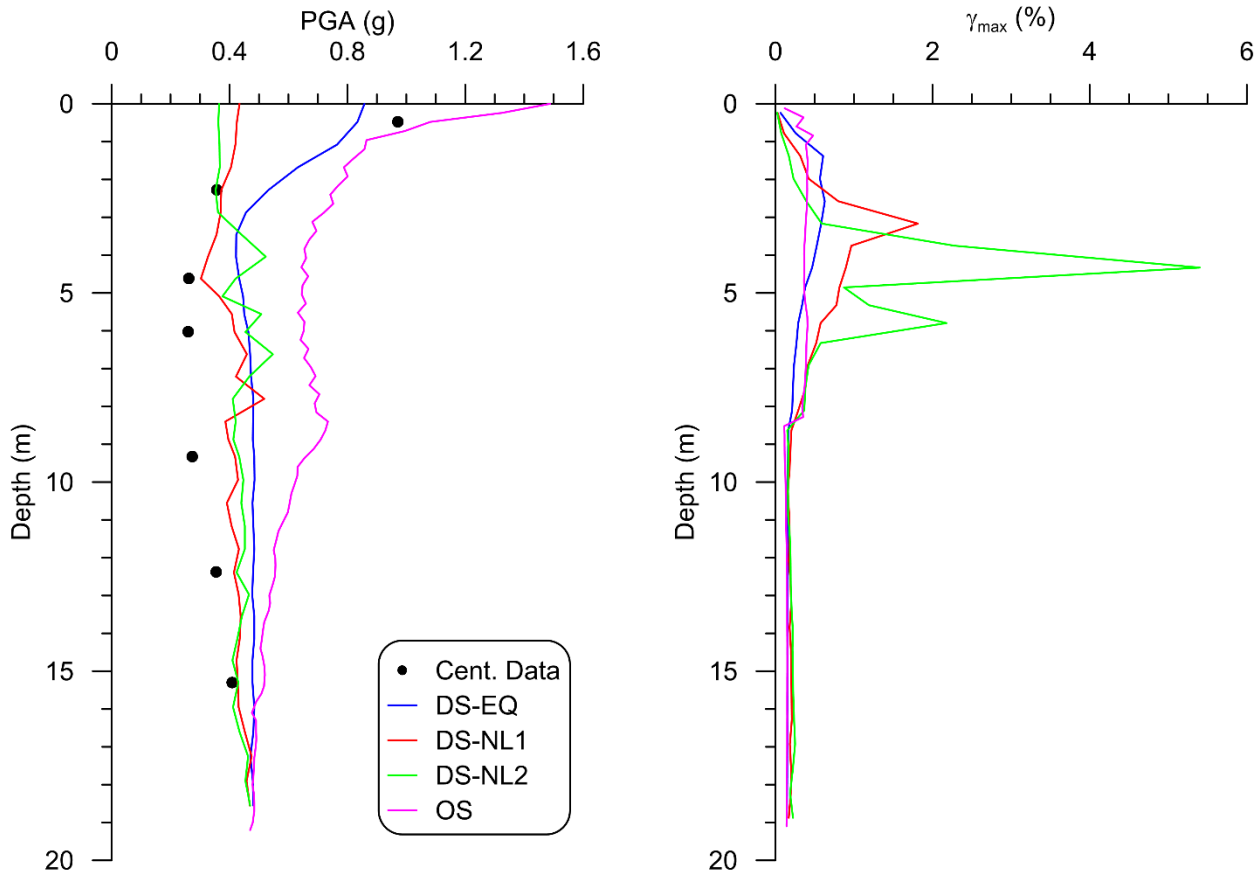

Figure 34. Profiles of peak acceleration and shear strain for various modeling approaches.

3 Summary and Conclusions

This report compared site response simulation results with centrifuge test measurements. Total stress analysis procedures were compared with centrifuge models of soft clay that were shaken with strong enough ground motion to induce strains higher than 10%, resulting in shear failure of the soil. Parameter variations in the site response simulations included the modeling approach (equivalent linear versus nonlinear), shear strength of the soil including corrections for strain rate effects, and nonlinear modeling platform (DeepSoil versus OpenSees).

The most important conclusions drawn from the total stress site response simulations presented in this chapter are as follows:

- Accurately modeling the shear strength of the soft clay was crucial to obtaining accurate ground motion predictions. The large-strain portion of the modulus reduction curve should be adjusted to obtain a desired shear strength, and the functional form of the modulus reduction equations (experimentally calibrated to strains only up to about 0.3%) should not be extrapolated to large strain. Yee et al. (2013) suggest a procedure for adjusting the modulus reduction curve to obtain a desired strength profile.
- Shear strain rate played a crucial role in increasing the shear strength mobilized during the centrifuge tests, and should be included in nonlinear site response simulations. Mobilized shear stresses exceeded monotonic undrained shear strengths by more than a factor of two due to the very large mobilized strain rates (as high as 6000%/s). Although model scale strain rates in the centrifuge are significantly higher than those anticipated at an equivalent prototype site (strain rate scales with centrifugal acceleration, in this case 57g), very large strain rates would also be anticipated under more realistic shaking conditions. The procedure suggested by Sheahan et al. is calibrated over typical laboratory strain rates, and extrapolation of this procedure resulted in an under-prediction of strength at high strain rates. However, this procedure appears to be suitable for strain rates that would be anticipated for field shaking conditions that mobilize strain rates lower than in centrifuge models due to centrifugal time scaling factors. More research is required to obtain strain rates for the range anticipated during earthquake shaking at soft soil sites.
- Nonlinear site response simulations utilizing the correct shear strength profile provided the most accurate results. Bias in model predictions that utilize an incorrect strength profile increases as

shaking intensity increases. However, bias is present for small input motions as well because the strength correction adjusts the modulus reduction curves at strains as small as 0.1%.

- Equivalent linear simulations can be adjusted to reasonably capture the peak response during any particular ground motion, but the amplitude and phase of these simulations were found to differ significantly from the data for smaller cycles. This is caused by the assumption that the strain-compatible modulus and damping values do not change in time, whereas in reality the secant modulus and damping evolve during shaking because strain amplitude also evolves.

Effective stress site response models were compared with centrifuge test data for a soil profile consisting of medium dense sand overlying dense sand. The model was shaken with a sequence of ground motions that generated large excess pore pressures in the model, resulting in liquefaction of the medium dense layer. High amplitude, high frequency acceleration pulses propagated through the liquefied soil profile due to the dilatant response of the sand in undrained loading. The models were analyzed using various nonlinear site response procedures and an equivalent linear site response method.

The primary conclusions from this section of the report are as follows:

- Ground motion records in liquefiable soils from field measurements and laboratory modeling studies indicate that liquefiable sand can propagate significant seismic energy in the form of high frequency pulses caused by the dilatant tendency of the sand being suppressed in undrained loading.
- Two classes of nonlinear effective stress site response modeling were studied: (1) pore pressure generation models that degrade the backbone stress-strain curve stiffness, and result in monotonic increases in excess pore pressure, and (2) advanced constitutive models that capture the tangent stiffening in the stress-strain behavior associated with the dilatant tendency of the sand being suppressed in undrained loading.
- Pore pressure generation models are incapable of capturing the transient stiffening associated with dilatancy in liquefiable deposits, and therefore fail to capture the acceleration pulses that propagate through liquefied sand. These models predict a "base isolator" effect in which surface motions are significantly reduced by the formation of a single layer that liquefies and reflects seismic energy downward. The "base isolator" effect is not supported by measurements of ground motions in liquefiable soils, and these models should not be used to predict post-liquefaction ground motions. In fact, the equivalent linear simulations predicted post-liquefaction ground motion better than these effective stress models.

- Advanced constitutive models that capture the dilatant tendency of liquefiable sands are capable of producing acceleration pulses similar to those observed in real ground motions in liquefiable soils. Although the model studied in this report qualitatively was able to capture the acceleration pulses, the amplitude of the pulses was not perfectly captured. More research will be required to resolve this issue.
- All of the nonlinear effective stress models accurately predicted liquefaction triggering of the centrifuge model. Hence, the pore pressure generation models may be useful for modeling triggering of liquefaction, but post-liquefaction ground motions were significantly unconservative.

4 Acknowledgments

We would like to thank former UCLA MS student Alek Harouonian and the NEES@UCDavis personnel, including Dan Wilson, Ross Boulanger, Bruce Kutter, Chad Justice, Ray Gerhard, Peter Rojas, Lars Pederson, Anatoliy Ganchenko, and Jenny Chen for their assistance during the centrifuge modeling. We would like to thank Youssef Hashash for his input related to DeepSoil modeling.

5 References

Afacan, K.B., Brandenberg, S.J., and Stewart, J.P. (2014). "Centrifuge Modeling Studies of Site Response in Soft Clay over Wide Strain Range.", Journal of Geotechnical and Geoenvironmental Engineering, 140(2), 04013003

Bolton, M. D. "The strength and dilatancy of sands." Geotechnique 36.1 (1986): 65-78.

Booker, John R., M. Shamimur Rahman, and Harry Bolton Seed. "GADFLEA: A computer program for the analysis of pore pressure generation and dissipation during cyclic or earthquake loading." Unknown 1 (1976).

Boulanger, Ross W., and Stephen P. Truman. "Void redistribution in sand under post-earthquake loading." Canadian geotechnical journal 33.5 (1996): 829-834.

Boulanger, R.W., and Ziotopoulou, K. (2012). "PM4Sand (Version 2): a sand plasticity model for earthquake engineering." Department of Civil and Environmental Engineering, University of California, Davis, Report. No. UCD/CGM-12/01, 101p.

Brandenberg, S.J., Boulanger, R.W., Kutter, B.L., and Chang, D. (2005). "Behavior of pile foundations in laterally spreading ground during centrifuge tests." J. Geotech. Geoenviron. Eng., ASCE., 131(11), 1378-1391.

Brandenberg, S.J., Stewart, J.P., Afacan, K.B., Harounian, A., Deng, L., and Park, D. (2010). "Final Report for USGS Award Number 08HQGR0037: Evaluation of nonlinear site response of soft clay using centrifuge models." United States Geological Survey. 33pg

Dafalias, Y.F., and Manzari, M.T. (2004). "Simple plasticity sand model accounting for fabric change effects." *J. Engineering Mechanics*, ASCE, 130(6), 622-634.

Darendeli, M. B. (2001). "Development of a new family of normalized modulus reduction and material damping curves." Ph.D. thesis, Univ. of Texas, Austin, TX.

Elgamal, A., Yang, Z., Parra, E., and Ragheb, A. (2003). "Modeling of cyclic mobility in saturated cohesionless soils." *International Journal of Plasticity*, 19(03) 883-905.

Green, R.A., Mitchell, J.K. and Polito, C.P. (2000). "An Energy-Based Pore Pressure Generation Model for Cohesionless Soils", Proceedings: John Booker Memorial Symposium, Melbourne, Australia, November 16-17, 2000.

Holzer, Thomas L., and T. Leslie Youd. "Liquefaction, ground oscillation, and soil deformation at the Wildlife Array, California." Bulletin of the Seismological society of America 97.3 (2007): 961-976.

Kayen, Robert, et al. "Geoengineering and seismological aspects of the Niigata-Ken Chuetsu-Oki earthquake of 16 July 2007." Earthquake Spectra 25.4 (2009): 777-802.

Kwok, A.O., Stewart, J.P., Hashash, Y.M.A., Matasovic, N., Pyke, R., Wang, Z.,and Yang, Z. (2007)."Use of exact solutions of wave propagation problems to guide implementation of nonlinear seismic ground response analysis procedures." *J. Geotech. & Geoenv. Eng.*, ASCE, 133 (11), 1385-1398.

Kutter, Bruce L., and Daniel W. Wilson. "De-liquefaction shock waves." Proc., 7th US–Japan Workshop on Earthquake Resistant Design of Lifeline Facilities and Countermeasures Against Soil Liquefaction, Rep. MCEER-99. Vol. 19. 1999.

Martin, G.R., and Qiu, P., 2001, “Site Liquefaction Evaluation: The Application of Effective Stress Site Response Analyses,” draft technical report prepared for the Multidisciplinary Center for Earthquake Engineering Research, Buffalo, NY.

Matasovic, N. (1992) “Seismic response of composite horizontally-layered soil deposits.” Ph.D. Thesis, University of California, Los Angeles.

Park, D., and Y. M. A. Hashash (2004) "Soil damping formulation in nonlinear time domain site response analysis," Journal of Earthquake Engineering, Vol. 8, No. 2, pp 249-274.

Polito, Carmine P., Russell A. Green, and Jongwon Lee. "Pore pressure generation models for sands and silty soils subjected to cyclic loading." Journal of Geotechnical and Geoenvironmental Engineering 134.10 (2008): 1490-1500.

Seed, Harry Bolton, Philippe P. Martin, and John Lysmer. The generation and dissipation of pore water pressures during soil liquefaction. College of Engineering, University of California, 1975.

Seed, H.B., De Alba, P.M., 1986. Use of SPT and CPT tests for Evaluating the Liquefaction Resistance of Sands. Proc., INSITU'86. ASCE Spec. Conf. on Use of In Situ testing in Geotechnical Engg., Spec. Publ. No. 6. ASCE, New York, N.Y.

Sheahan, T., Ladd, C., and Germaine, J. (1996). ”Rate-dependent undrained shear behavior of saturated clay.” *J.Geotech. & Geoenviron. Eng.*, ASCE, 122 (2), 99–108.

Wilson, D.W., Boulanger, R.W., and Kutter, B.L. (2000). "Observed seismic lateral loading resistance of liquefying sand." *J. Geotech. Geoenviron. Eng.* 126(10), 898-906.

Yee, E, JP Stewart, and K Tokimatsu (2013). “Elastic and large-strain nonlinear seismic site response from analysis of vertical array recordings,”J. Geotech. Geoenviron. Eng., 139 (10), 1789-1801.

Yong, R. N., and R. D. Japp. "Stress-strain behavior of clays in dynamic compression." Vibration effects of earthquakes on soils and foundations, ASTM Special Technical Publication 450 (1969): 233-262.